Supercurrent noise in rough Josephson junctions

by

Pierre-Luc Dallaire-Demers

A thesis
presented to the University of Waterloo
in fulfillment of the
thesis requirement for the degree of
Master of Science
in
Physics

Waterloo, Ontario, Canada, 2011

I hereby declare that I am the sole author of this thesis. This is a true copy of the thesis, including any required final revisions, as accepted by my examiners.

I understand that my thesis may be made electronically available to the public.

Abstract

Josephson junctions are dissipationless elements used notably in superconducting nanocircuits. While being indispensable for the making of superconducting quantum bits, they are plagued by intrinsic noise mechanisms that reduce the coherence time of the quantum devices. An important source of such fluctuations may come from the non-cristallinity and disorder of the oxide layer sandwiched between the two superconducting leads. In this work, roughness in a Josephson junction is modeled as a set of pinholes with a universal bimodal distribution of transmission eigenvalues that sum incoherently in the noise power. Each of these channels is treated as a ballistic quantum point contact with a thin barrier that determines the transmission eigenvalue. The noise spectrum is calculated using the quasi-classical Green's function method to analyze high and low transmission limits at non-zero temperature for all interesting frequencies. As suggested by experiments, low transmission channels generate shot noise while fast switching between subgap states creates strong non-poissonian low-frequency noise. However, when analyzed for three different universal models of disorder, the principal contribution to noise is found to come from the partially opened channels. Finally, fluctuations of the noise from sample to sample is seen to be dominated by the contribution of opened channels which may reduce the reproducibility of results between different experiments.

Acknowledgements

I would first like to offer my gratitude to my supervisor Frank Wilhelm-Mauch for his patience in enduring my varying levels of productivity and for his willingness and enjoyment in sharing his vast and sharp knowledge of physics. I always enjoy his sense of humour and his innumerable anecdotes surrounding the physics community. He serves as a model for me and others and I am truly blessed to have him as my supervisor for my graduate studies.

I also want to offer my thanks to Mohammad Ansari for his precious help in solving many intricate problems during the course of my master and for sharing insights on the art of doing physics that kept challenging my views on the field.

I wish to highlight the contributions of my thesis committee members for their patient work. Adrian Lupascu was willing to share thoughtful advices on the experimental implications of my research, Elisabeth Nicol was teaching the wonders of physics with a contagious cheerfulness and enjoyment and Anton Burkov accepted a last minute invitation to join the committee and review my work.

I would like to thank all the members (and ex-members) of the Quantum Device Theory group Bothan, Peter, Felix, Wen Ling, Yuval, Luke, Farzad, Bill, Georg, Seth, Emily and Jay for everything I learnt from them. I am truly lucky to be working with such smart people. I also enjoyed good discussions and fun times with members from Adrian's group and other IQC students which are too numerous to list here. I express special thanks to the IQC staff who made my life in Waterloo simpler, especially Andrew whose work saved me a lot of administrative headaches.

On a personal side I must thank François and Florence for never giving up in helping me become a better person. There could be no better friends. I also raise my hat to everyone gravitating around the de Rouen commune, these are extraordinary people.

Finally I would like to thank my parents Marc and Céline as well as my sisters Claudia and Gabrielle. There is no better driving force than their love and presence.

This works was financially supported by the Natural Sciences and Engineering Research Council of Canada, the Fonds de recherche du Québec - Nature et technologies and the Intelligence Advanced Research Projects Activity funding agencies.

Table of Contents

List of Figures

Chapter 1

Introduction

1.1 Quantum Computing with Superconducting Qubits

A quantum bit (qubit) [1] is the fundamental unit of quantum information. As a classical bit can be either in the state 0 or 1, the state $|\psi\rangle$ of a qubit can be represented as a pure superposition of computational states

$$|\psi\rangle = \alpha\,|0\rangle + \beta\,|1\rangle \tag{1.1}$$

where $|\alpha|^2 + |\beta|^2 = 1$. Universal quantum computation relies on the ability to implement any unitary operator U on an initial state and take it to a desired final state.

$$|\psi\,(t)\rangle = U\,(t, t_0)\,|\psi\,(t_0)\rangle\,. \tag{1.2}$$

However, the pure state description of the system may not be complete if there is uncertainty in the preparation of the state. If we are given a system that has been prepared in a state ψ_i with probability p_i, then we can fully describe the ensemble of possible states as a density operator

$$\rho = \sum_i p_i\,|\psi_i\rangle\,\langle\psi_i|. \tag{1.3}$$

Given the density operator of a system, the amount of quantum information it contains can be measured using Von Neumann's entropy formula:

$$S\,(\rho) = -\mathrm{tr}\,(\rho \log \rho)\,. \tag{1.4}$$

This definition of the entropy implies that a pure state has no entropy and can be used as a resource for quantum computing. On the contrary, Von Neumann's entropy is maximal if nothing is known about the given state. In the case of a fully mixed state, its density operator is simply the unit matrix, which is invariant with respect to unitary transformations. Decoherence corresponds to an increase of the entropy of an open quantum system when it leaks information to its environment.

The technological challenge of implementing a physical quantum computer [2] has been divided in five objectives by DiVincenzo. To be used as a general purpose quantum computer, a system should:
1. Have well defined addressable qubits
2. Be initializable to a pure state
3. Have access to a universal set of quantum gates
4. Allow the measurement of any qubit
5. Have a coherence time much longer than any gate implementation or measurements.

A promising technology for the implementation of quantum computers are superconducting nanocircuits. Superconducting materials are characterized by two important properties [3]: below a certain critical temperature they exhibit dissipationless current and they expel all magnetic field from their bulk. While dissipationless currents means that no information should leak out of a circuit in the form of resistive heating, the later property, known as the Meissner effect, allows flux and fluxoid quantization which is a fundamental effect used by SQUIDs.

Furthermore, superconducting circuits have several other advantages. The fabrication of micrometre to centimetre sized circuit is a very mature technological field requiring relatively basic equipment to manufacture compared to modern semiconductors. Also, the microscopic physics of simple superconductors has been well established for more than 50 years. The Bardeen-Cooper-Schrieffer (BCS) theory of Cooper pairing where electrons in a metal pair up through an attractive phonon interaction explains all properties of conventional superconductors. The paired electrons form a new collective ground state with an energy lower than the usual Fermi surface. This collective state can be characterized by an amplitude and a phase such that $\psi(\mathbf{r},t) = |\psi(\mathbf{r},t)|\, e^{i\phi(\mathbf{r},t)}$. Let's note that this wave function oscillates on a scale which is much larger than the lattice spacing of the material, implying that superconductivity can be seen as a macroscopic quantum phenomenon. Supercurrent in superconductors is explained by the centre-of-mass movement of the collective state which is left invariant by the individual scattering of electrons on impurities, the mechanism inducing resistivity in normal metals. Supercurrent is not carried by low-energy excitations but is rather an equilibrium phenomena where the collective state acquire a

spatially oscillating phase through a Galileo transformation. The effective charge of the Cooper pairs carrying the current is twice the charge and mass of the electron and has zero spin. Dissipative quasiparticles are separated from the condensate by an energy gap $\Delta = 1.76 k_B T_c$, where T_c is the critical temperature of the superconductor. Therefore to operate a superconducting device, the temperature must be lowered far below T_c and the system must be electrically isolated from the environment to minimize dissipation. As we'll show in the following part, the dissipationless current can be used in principle to make qubits with long coherence times.

1.1.1 Superconducting Nanocircuits

There are three important passive building blocks of superconducting circuits. While there are no resistors, there are inductors, capacitors and Josephson junctions, which are the characteristic elements of superconducting circuit. Josephson junctions are tunnel junctions coupling two superconductors with arbitrary phases with and intermediate insulating layer usually 2 to 3 nm thick. The spatial variation of the phase imposes a finite group velocity of the condensate, which translate as an equilibrium supercurrent without applying any voltage difference across the junction. If we know the gauge invariant phase difference across the junction, the supercurrent is given by the first Josephson relation

$$I = I_c \sin(\phi). \tag{1.5}$$

The critical current I_c can be computed at finite temperature T using the Ambegaokar-Baratoff formula if we know the normal state conductance of the junction G_N and the gap Δ of the superconductor:

$$I_c = \frac{\pi G_N \Delta}{2e} \tanh\left(\frac{\Delta}{2\mathrm{k_B T}}\right). \tag{1.6}$$

Let's note that the phase difference across a Josephson junction can be by applying a voltage difference V. This effect is described by the second Josephson relation

$$\hbar\dot{\phi} = 2eV. \tag{1.7}$$

If we were to use conventional LC resonators to build qubits, the harmonic spectrum would make the proper addressability of qubits impossible as all transitions of an harmonic oscillator have the same energy. The inclusion of Josephson junction as non-linear inductance allows one to engineer non-quadratic potentials which lift the degeneracy of level transitions. Therefore Josephson junctions are key elements if one endeavor to build a practical quantum computer out of superconducting nanocircuits.

The allowed energy states of a classical circuit form a continuum. To implement quantum processing devices, well resolved discrete energy states are required. Since the electrons in a superconductor behave as a single collective state, Schrödinger's equation describes the dynamic of the circuit and discrete energies eigenstates can be found if the temperature is low enough.

Here is an overview of the procedure to quantize the energy levels of an electrical circuit. First write the Kirchhoff laws and extract an equation of motion as a function of the flux Φ and its first time derivative. From this a Lagrangian can be found and transformed to a Hamiltonian form from which we can proceed to do canonical quantization with the appropriate commutation relation. Finally the energy spectrum can be solved from Schrödinger's time-independent equation. If a Josephson junction is present, the current in Kirchhoff law is found from formula 1.5 using $\phi = 2\pi\frac{\Phi}{\Phi_0}$. If several junctions are used then the phases are found from fluxoid quantization.

1.1.2 Examples of Qubit Design

Three important circuit topologies have been developed to implement superconducting qubits, namely the charge qubit, the flux qubit and the phase qubit [4].

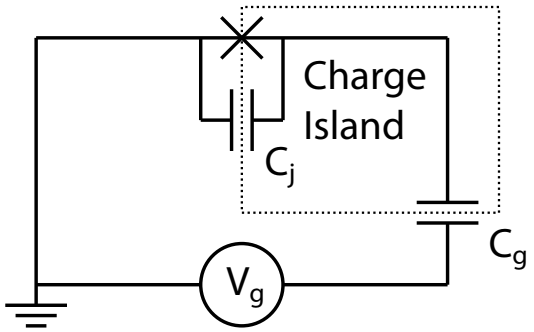

Figure 1.1: Circuit diagram of a charge qubit. The cross corresponds to the Josephson junction. C_j is the junction capacitor and C_g is the gate capacitor. The number of Cooper pairs on the island is controlled by the gate voltage V_g.

Charge qubit

An example of a charge qubit circuit is shown in figure 1.1. In a charge qubit, the degree of freedom encoding the computational state is the number of Cooper pairs on a superconducting island formed between a gate capacitor C_g and a Josephson junction. By varying

the gate voltage V_g, Cooper pairs can tunnel in and out the the island. Once extracted with the method from the previous subsection and expressed in the charge representation, the Hamiltonian of the charge qubit describe well this situation:

$$H = E_c \left(n + n_g\right)^2 - \frac{E_J}{2} \sum_n \left(|n\rangle \langle n+1| + |n+1\rangle \langle n|\right). \tag{1.8}$$

In this Hamiltonian, $E_C = \frac{2e^2}{C_g + C_j}$ is the charging energy and $E_J = I_c \frac{\Phi_0}{2\pi}$ is the Josephson energy. Furthermore, $n = \frac{Q}{2e}$ is the discrete number of excess pairs on the island while $n_g = \frac{C_G V_G}{2e}$, a continuous classical variable, is the gate voltage in units of charge number. Charge qubits require that $E_C \gg E_J$ in such a way that the number of Cooper pairs on the island is fixed around a certain value and the tunnelling rate is controlled by the ratio of the junction area over its thickness. There exists a useful operating point at $n_g = n + \frac{1}{2}$ in the energy diagram of the charge qubit such that small fluctuations of the gate voltage will only induce second order fluctuations of the number of charges on the island. At this "sweet spot" there are two energy wells separated from lower and higher energy levels, in this case the Hamiltonian takes the simplified form

$$H_{SP} = \begin{pmatrix} E_C n_g^2 & \frac{E_J}{2} \\ \frac{E_J}{2} & E_C \left(n_g + 1\right)^2 \end{pmatrix}. \tag{1.9}$$

It can be noticed that if the Josephson energy was to fluctuate, it would create undesired transitions between the energy levels and increase the entropy of the qubit. Finally, measuring the charge on the island can be done directly with a single-electron transistor or dispersively by coupling the qubit to a cavity.

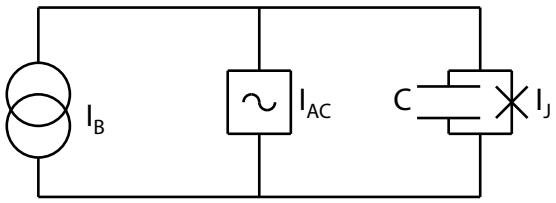

Figure 1.2: Circuit diagram of a phase qubit. A bias current I_B creates an effective tilted washboard potential in the Josephson junction (cross) and an alternating current source I_{AC} drives transitions between the qubit's levels.

Phase qubit

An example of a phase qubit is shown in figure 1.2. In this device, the quantum information

is encoded in the phase ϕ degree of freedom of a Josephson junction. By biasing the junction at a given current I_B, the equation of motion of ϕ obtained is analogous to the one of a particle in a tilted washboard potential, where the phase is represented by the position of the particle and the capacitance C by its mass. In the representation where ϕ and the charge Q are conjugate variables $[\phi, Q] = 2ie$, the Hamiltonian takes the form

$$H = \frac{Q}{2C} - E_J \cos(\phi) - I_B \frac{\Phi_0}{2\pi}\phi. \tag{1.10}$$

If the current bias and the junctions parameters are chosen appropriately, the potential can be made such that the solution to the Schrödinger equation has only 3 to 6 bound states in each potential well at $\phi = \frac{\pi}{2}$. The plasma oscillation frequency of the lowest levels of those wells is given by

$$\omega_p(I) = 2^{\frac{1}{4}} \left(\frac{2\pi I_0}{\Phi_0 C}\right)^{\frac{1}{2}} \left(1 - \frac{I}{I_0}\right)^{\frac{3}{2}}. \tag{1.11}$$

Those levels have different transition frequencies, which means they can be addressed individually using an alternating current source I_{AC}. The computational states are usually chosen to be the ground state and the first excited state. Measurements can be done by lowering the potential barrier such that the ground state probability of tunnelling stays low but higher energy states quickly tunnel through the barrier, producing a stream of quasiparticles and a voltage spike in accordance with the second Josephson relation. We note that the potential barrier height is given by

$$\Delta U(I) = \frac{2\sqrt{2}}{3\pi} I_0 \Phi_0 \left(1 - \frac{I}{I_0}\right)^{\frac{3}{2}}. \tag{1.12}$$

Let's remark that fluctuations of the critical current I_c modulate the barrier height which has two possible effects. It broadens the levels of the qubit, which produces dephasing, and it raises the chance of tunnelling out of the potential well, reducing the lifetime of the qubit.

Flux qubit

An example of a third type of qubit, the flux qubit, is shown in figure 1.3. In this case, the quantum information is encoded in states of clockwise and counterclockwise currents. The flux Φ is such that the frustration of the loop

$$f = 2\pi \frac{\Phi}{\Phi_0} = \pi, \tag{1.13}$$

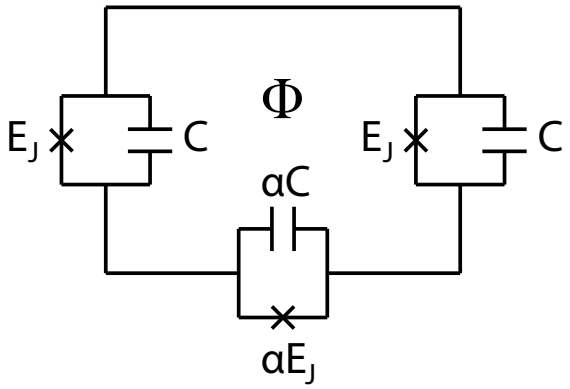

Figure 1.3: A circuit diagram of a flux qubit is shown. A loop with three Josephson junctions is threaded by a flux Φ. The smaller junction is made such that α is around 0.8. The self-inductance of the loop must be much smaller than the inductance of the junctions.

which means from fluxoid quantization that the sum over the phase of all junctions must be equal to π. This is such that clockwise and counterclockwise states of currents have the same energy. If the charging energy $E_C < E_J$ by a factor of about 40 to 80 and α is around 0.8, then the energy barrier between the two states becomes small enough to allow tunnelling between the opposing states of current. The tunnel coupling Δ can be found from a WKB calculation. This coupling implies that there exists a ground state with a symmetric superposition of opposing currents and an excited state with an antisymmetric superposition of currents. In its ground state, the system naturally implement a NOT gate by cycling between states of opposing currents. By varying the frustration, we lift the degeneracy between the clockwise and the counterclockwise currents, which creates a Z gate. In the computational basis, the Hamiltonian is therefore

$$H = \frac{1}{2}\begin{pmatrix} I_p\left(\Phi - \frac{\Phi_0}{2}\right) & \Delta \\ \Delta & -I_p\left(\Phi - \frac{\Phi_0}{2}\right) \end{pmatrix}, \tag{1.14}$$

where I_p is the magnitude of the opposing currents which are created by the small junction whose phase $\phi = \pi \pm \epsilon$. The qubit state can be measured with a SQUID which collapses the system to one of its classical states of current. We notice that if there are current fluctuations in the Josephson junctions, this can create energy fluctuations and induce dephasing. Also, since the critical current also modulates the height of the coupling barrier, current fluctuations could produce undesired transitions between the levels of the flux qubit.

If we analyze superconducting qubits in the light of DiVincenzo's criteria, we find that,

using Josephson junctions, non-harmonic potentials with a few well defined levels can be created. At very low temperature $E_C, E_J \gg k_B T$, qubits in thermodynamic equilibrium are in their ground state, they can therefore be initialized. Gate implementations are well mastered and can be very precise. Superconducting qubits can be coupled together. Measurements can be done with a good fidelity. However, the qubits lifetime are not yet sufficiently long to use them as memory. This is caused by decoherence for which a possible cause is explored in the next subsection.

1.2 Current Fluctuations in Superconducting Qubits

The technology of superconducting qubits is evolving fast. However, we still haven't reached the point where we can do universal quantum computing with these devices. Their limited lifetimes is currently the major source of errors during their operations as quantum information processing devices. Despite their superconducting nature, they still dissipate energy to the environment, which brings them back quickly to their ground state in a characteristic time T_1. Other unwanted interactions with the environment or control errors may also be causing dephasing by making the qubits' Hamiltonians fluctuate. However, the qubits' lifetimes do not have to be infinite to do universal quantum computation. Indeed, if the error rate reaches below a certain threshold, fault-tolerant control schemes can be implemented and we can then proceed with arbitrarily long computations. This is why sources of decoherence must be identified and engineered out.

Several sources of decoherence are being investigated. For example, noise and dissipation may come from the Purcell effect, from dielectric losses, from sources of dissipative quasiparticles, from flux noise, from surface defects interacting with the electron condensate or from current fluctuations. In our case, we focus on current fluctuations and their effect on the decoherence of superconducting qubits. Previous works on the subject [5] [6] [7] [8] [9] [10] have been done for junctions at zero-frequency and finite voltage and for quantum point contacts at finite frequency, but never for junctions at finite frequency and vanishing voltage, which is the regime of operation of superconducting qubits.

At finite frequency ω, what are the possible sources of current fluctuations? At finite temperature T there may be transitions between the internal states of the junctions responsible for charge transport. These states are called Andreev reflections, they are the mechanism by which supercurrent is transformed into normal current in the junction's oxide layer. In a SNS structure, Andreev reflections going in and out of the normal layer form a pair of bound states responsible for the Josephson effect. Unwanted thermal transitions between these bound states may be a cause of current fluctuations. Furthermore, these

bound states may have an imaginary part to their self-energy caused by electron-phonon interactions or impurity scattering. Transitions within these energy bands may also be sources of current fluctuations. Also, since the physics of Andreev reflection is strongly dependent on the value of the transmission eigenvalues composing the junction, disorder and chaotic transport may have an effect on the current noise spectrum. Disorder itself may take different forms. It can come from the roughness of the junction, from its geometry or from the quality of the crystal lattice. In this work, we will take a closer look at the contributions to the noise spectrum by these sources of disorder. An analysis of their impact on the sample-to-sample noise fluctuations will also be provided.

1.2.1 Measuring the Noise Spectrum with a Qubit

A qubit can be used as a spectrometer to experimentally access the noise spectrum of one of its parameters [11]. To measure classical noise, we select a specific frequency to analyze with a resonant circuit. The signal is then amplified and a square law detector such as a diode rectifier measures the square amplitude of the noise at the chosen frequency.

Superconducting nanocircuits operating in the GHz frequency range and a few tens of millikelvins enter a regime where $\hbar\omega > k_B T$ for which quantum noise has to be measured with quantum amplifiers and quantum detectors. While thermal noise in a resistor may vanish at low temperature when thermal fluctuations progressively reach zero, quantum fluctuations however remain even at $T = 0$. To measure the zero point motion of the noise, a quantum system may be used. The spontaneous decay rate of such a system contains information about the noise spectrum even at zero temperature. For non vanishing temperatures, the spectrum will also contain blackbody radiation where stimulated emission and absorption rates additional yield information about the noise spectrum.

Let's suppose we have a two-level system with an Hamiltonian

$$H = -\frac{\hbar\Omega}{2}\sigma_z, \tag{1.15}$$

where Ω is a tunable frequency. An external noise source induces transitions of the two-level system. The transition rate gives information on the amplitude of the noise at the particular frequency Ω. The noise source with amplitude $f(t)$ is modeled as a transition-inducing perturbation

$$V = Af(t)\,\sigma_x, \tag{1.16}$$

where A is the coupling constant to the measuring system. We suppose that initially the system is prepared in its ground state and left to evolve freely under the perturbation until

time t where its state is measured. First-order time-dependent perturbation theory can be used to compute the average time evolution of the system. It is assumed that the noise correlation function is stationary and has a small autocorrelation time $\tau_F \ll t$. The noise spectral density is defined as

$$S_f(\omega) = \int_{-\infty}^{\infty} dt e^{i\omega t} \langle f(t) f(0) \rangle. \tag{1.17}$$

The correlation function can be computed from first principles using the Green's function method and it connects to different measurable quantities in experiments. One of those cases is the transition rate if the system is initially in the ground state

$$\Gamma_{\uparrow} = \frac{A^2}{\hbar^2} S_f(-\Omega). \tag{1.18}$$

Alternatively if the system is initially in the excited state we get

$$\Gamma_{\downarrow} = \frac{A^2}{\hbar^2} S_f(\Omega). \tag{1.19}$$

For example, a resistor can be modeled as a set of harmonic oscillators in series [11]. Its voltage fluctuations are given by

$$S_V(\omega) = \frac{2R_0\hbar\omega}{1 - e^{-\frac{\hbar\omega}{k_B T}}}. \tag{1.20}$$

At high temperature we obtain the Johnson noise $S_V(\omega) = 2R_0 k_B T$ while in the quantum limit we get $S_V(\omega) = 2R_0\hbar\omega\Theta(\omega)$ where energy can only be absorbed. Another connection of the noise spectral density with experiments is the steady-state polarization of the qubit given by

$$P_{ss} = \frac{\Gamma_{\downarrow} - \Gamma\uparrow}{\Gamma_{\downarrow} + \Gamma\uparrow}. \tag{1.21}$$

If the system's polarization is in a non-equilibrium state, then the relaxation rate to the steady state is given by

$$\Gamma_1 = \frac{1}{T_1} = \Gamma_{\downarrow} + \Gamma_{\uparrow}. \tag{1.22}$$

So to fully describe quantum noise we need either the full spectrum at negative and positive frequencies or the polarization and T_1, which contain information on both the antisymmetric and symmetric part of the noise.

From there, sample-to-sample fluctuations of the noise can easily be accessed by computing the root mean square of the noise found for an ensemble of similar device.

1.2.2 Overview of the Theoretical Method

In chapter 2, we will compute the noise spectrum for an arbitrary superconducting channel. This will provides insights on the mechanisms of current noise involving thermal transitions between the microstates of a junction and give us a building block to analyze the effect of disorder in Josephson junctions in chapter 3.

Since finite frequency noise at finite temperature involves absorption and emission of energy inside a Josephson junction, it has to be treated with non-equilibrium methods of many-body physics. The Keldysh formalism is the appropriate tool to tackle the problem and it will first be introduced. Also, since transport in superconducting system is especially related to the physics of states near the Fermi surface, the quasiclassical method for Green's functions will be introduced briefly.

After we will describe the model of a SNS channel and find the complete form of the Green's functions which are solutions to the Gor'kov equation in this model. From there, numerical tools are used to compute the noise for a channel at arbitrary frequency, temperature, relaxation rate, phase and transparency. We will vary these parameters and analyze their effects on the current noise in regimes similar to those of superconducting qubits.

In the last chapter we will use that knowledge to compute the average noise and the sample-to-sample noise fluctuations of disordered structures like diffusive wire, chaotic cavities and dirty interfaces. These structures model different types of Josephson junctions. Their similarities and differences will be highlighted.

Chapter 2

Non-equilibrium Transport in Josephson Junctions

2.1 Keldysh Formalism

2.1.1 General Concepts

The many-body Green's function method is a powerful tool of condensed matter physics[12][13]. The determination of the Green's function of a given system gives access to all its physical observables at equilibrium for any temperature. The effects of time independent interactions between particles of many-body systems can be computed using Feynman diagrams and a Dyson equation can be used to compute the perturbation expansion up to any desired order.

In the case where the disturbance of the system is time-dependent and produces transitions between the states of the system, other methods need to be employed. The standard linear response theory being only valid up to first order in the disturbance, a more general Green's function approach is required to compute the effects of the perturbation up to any order. The tool for this job is the nonequilibrium Green's function method which uses several Green's functions to characterize a contour along the real time axis instead of the standard time-ordering procedure. Its most elegant form being the Keldysh formulation, we proceed to show in this section how the new Green's functions are defined and how they can be applied to problems involving superconductivity.

The standard method [14] to obtain a nonequilibrium state is to first consider an ensemble of interacting particles such that their time-independent Hamiltonian has the form

$H = H_0 + H^i$, where H_0 represents the free particles and H^i contains the information about their mutual interactions. The system is assumed to be in thermodynamic equilibrium until time t_0, where a disturbance $H'(t)$ is turned on such that the full Hamiltonian becomes $\mathcal{H}(t) = H + H'(t)$. The average value of an observable of interest can then be computed in the Heisenberg picture

$$\langle O_{\mathcal{H}}(t)\rangle = \mathrm{Tr}\left[\rho(\mathrm{H})\,\mathrm{O}_{\mathcal{H}}(\mathrm{t})\right]. \tag{2.1}$$

At equilibrium, the density matrix is known to be $\rho(H) = \frac{e^{-\beta H}}{\mathrm{Tr}\left\{\mathrm{e}^{-\beta \mathrm{H}}\right\}}$ from statistical mechanics and it is computable for quadratic Hamiltonians such as mean-field BCS. The grand canonical ensemble is used where particle energies are measured relative to the chemical potential μ.

The lesser and greater Fermionic Green's functions linking the measurable observables to the easily calculable quantities are defined as

$$\begin{aligned} G^{<}(1,1') &= i\left\langle \psi^{\dagger}_{\mathcal{H}}(1')\,\psi_{\mathcal{H}}(1)\right\rangle \\ G^{>}(1,1') &= -i\left\langle \psi_{\mathcal{H}}(1)\,\psi^{\dagger}_{\mathcal{H}}(1')\right\rangle \end{aligned}. \tag{2.2}$$

The notation where $1 \to \mathbf{r}_1, t_1$ is used. In principle, any single-particle operator can be expressed as a function of those Green's functions. A closed time path Green's function

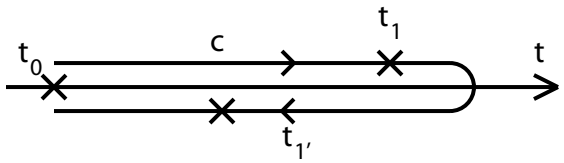

Figure 2.1: Closed time path contour c. The contour starts at t_0, goes to t and then comes back to t_0 by following the real axis.

with a simple perturbation expansion can be defined on the contour c shown in figure 2.1:

$$G(1,1') = -i\left\langle T_c\left[\psi_{\mathcal{H}}(1)\,\psi^{\dagger}_{\mathcal{H}}(1')\right]\right\rangle. \tag{2.3}$$

In this case, T_c orders the field operators according to the position of their time argument on the contour c such that

$$G(1,1') = \begin{cases} G^{>}(1,1') & t_1 >_c t_{1'} \\ G^{<}(1,1') & t_1 <_c t_{1'} \end{cases} \tag{2.4}$$

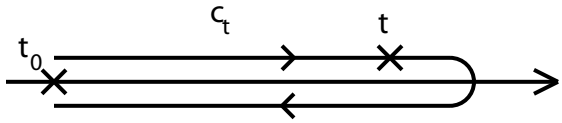

Figure 2.2: Transformation contour c_t. A single time argument starts and ends at t_0.

This new Green's function now contains all the information on $G^{>}$ and $G^{<}$. The operator $O_{\mathcal{H}}$ in the Heisenberg picture should now be represented as a function of O_H in the interaction picture with respect to H using

$$O_{\mathcal{H}}(t) = u^{\dagger}(t, t_0)\, O_H(t)\, u(t, t_0) \tag{2.5}$$

where

$$u(t, t_0) = T\exp\left(-\mathrm{i}\int_{\mathrm{t_0}}^{\mathrm{t}} \mathrm{dt'H'_H(t')}\right). \tag{2.6}$$

Here T is the usual time ordering operator and $H'_H(t)$ is $H'(t)$ in the interaction picture with respect to H. Equation 2.5 can be rewritten in the form

$$O_{\mathcal{H}}(t) = T_{c_t}\left\{\exp\left[-\mathrm{i}\int_{\mathrm{c_t}} \mathrm{d\tau H'_H(\tau)}\right] \mathrm{O_H(t)}\right\} \tag{2.7}$$

where c_t is the contour shown in figure 2.2. The Green's function in the interaction picture with respect to H is then given by

$$G(1, 1') = -i\left\langle T_c\left[S_c^H \psi_H(1)\, \psi_H^{\dagger}(1')\right]\right\rangle \tag{2.8}$$

where c is the contour shown in figure 2.1 and

$$S_c^H = \exp\left[-\mathrm{i}\int_{\mathrm{c}} \mathrm{d\tau H'_H(\tau)}\right]. \tag{2.9}$$

To use Wick's theorem, we must go in the interaction picture with respect to H_0 which is assumed to be quadratic with respect to the field operators. The following relation is used

$$e^{-\beta H} = e^{-\beta H_0} T\exp\left[-\mathrm{i}\int_{\mathrm{t_0}}^{\mathrm{t-i\beta}} \mathrm{dt'H^i_{H_0}(t')}\right], \tag{2.10}$$

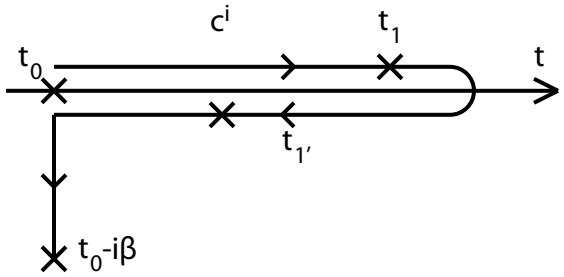

Figure 2.3: Interaction contour c^i. This contour is similar to figure 2.1 but it adds an imaginary part to account for the initial thermal equilibrium between the particles.

where $H^i_{H_0}(t)$ is H^i in the interaction picture with respect to H_0. We get

$$G(1,1') = -i\frac{\mathrm{Tr}\left[\mathrm{e}^{-\beta \mathrm{H}_0}\mathrm{T_c}\left(\mathrm{S_{c^i}S_c}\psi_{\mathrm{H}_0}(1)\,\psi^{\dagger}_{\mathrm{H}_0}(1')\right)\right]}{\mathrm{Tr}\left[\mathrm{e}^{-\beta \mathrm{H}_0}\mathrm{T_c}\left(\mathrm{S_{c^i}S_c}\right)\right]} \tag{2.11}$$

where

$$\begin{array}{l} S_{c^i} = \exp\left[-\mathrm{i}\int_{\mathrm{c^i}} \mathrm{d}\tau \mathrm{H}^{\mathrm{i}}_{\mathrm{H}_0}(\tau)\right] \\ S_c = \exp\left[-\mathrm{i}\int_{\mathrm{c}} \mathrm{d}\tau \mathrm{H}'_{\mathrm{H}_0}(\tau)\right] \end{array} \tag{2.12}$$

Let's note that c^i is the interaction contour shown in figure 2.3. Wick's theorem is valid for those contours, we can use it just as in equilibrium theory to extract Feynman diagrams of a perturbation expansion for G. Equilibrium and nonequilibrium statistical mechanics have the same form and structure, except that the later orders field operators around a contour instead of the usual time ordering procedure for the equilibrium case. In the density matrix formalism, the bra vectors are propagated backward from t to t_0 while the ket vectors are propagated in the forward time direction.

The part of the contour from t_0 to $t_0 - i\beta$ in figure 2.3 contains the information about the initial conditions which can be discarded and imposed directly on the integral form of the Dyson equation. We can let $t_0 \to -\infty$. Since the evolution operator is unitary, we can also set the largest time to $+\infty$ in such a way that the contours c and c^i becomes the same. This is the Keldysh contour a shown in figure 2.4 that extends from $-\infty$ to $+\infty$ in c_1 and then back from $+\infty$ to $-\infty$ in c_2.

The Green's function G_{c_K} defined on the Keldysh contour takes different values depending on the relative position of the time arguments t_1 and $t_{1'}$. It can therefore be mapped onto a matrix space such that

$$G_{c_K}(1,1') \longmapsto \breve{G} \equiv \begin{pmatrix} G_{11} & G_{12} \\ G_{21} & G_{22} \end{pmatrix}. \tag{2.13}$$

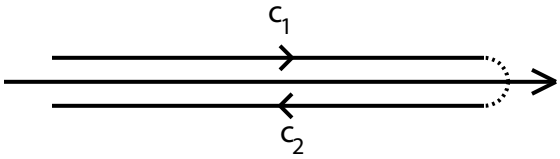

Figure 2.4: The Keldysh contour c_K run from $t = -\infty$ to $t = +\infty$ along the real time axis and then back again.

The time arguments t_1 and $t_{1'}$ of the $G_{ij}(1,1')$ respectively reside on c_i and c_j. The components can be written as

$$\begin{array}{rcl} G_{11}(1,1') & = & -i\left\langle T_{c_1}\left[\psi_{\mathcal{H}}(1)\,\psi^{\dagger}_{\mathcal{H}}(1')\right]\right\rangle \\ G_{12}(1,1') & = & G^{<}(1,1') \\ G_{21}(1,1') & = & G^{>}(1,1') \\ G_{22}(1,1') & = & -i\left\langle T_{c_2}\left[\psi_{\mathcal{H}}(1)\,\psi^{\dagger}_{\mathcal{H}}(1')\right]\right\rangle \end{array} \tag{2.14}$$

Since these components are not linearly independent, there exists a more convenient representation of G_{c_K} such that one-body coupling has the simplest possible form using standard and retarded Green's functions. Using the following identities

$$\begin{array}{rcl} G^{R}(1,1') & = & G_{11}(1,1') - G_{12}(1,1') \\ & = & G_{21}(1,1') - G_{22}(1,1') \\ G^{A}(1,1') & = & G_{11}(1,1') - G_{21}(1,1') \\ & = & G_{12}(1,1') - G_{22}(1,1') \\ G^{K}(1,1') & = & G_{21}(1,1') + G_{12}(1,1') \\ & = & G_{11}(1,1') + G_{22}(1,1'), \end{array} \tag{2.15}$$

the Green's function G_{c_K} can then be mapped onto the matrix $\check{G}$ such that

$$G_{c_K}(1,1') \longmapsto \check{G} \equiv \begin{pmatrix} G^{R} & G^{K} \\ 0 & G^{A} \end{pmatrix}. \tag{2.16}$$

In the case of superconducting transport, the standard field operator are replaced by the Nambu pseudospinor field $\hat{\psi} = \begin{pmatrix} \psi_{\uparrow} \\ \psi^{\dagger}_{\downarrow} \end{pmatrix}$. This implies that $\hat{G}^{R}$,$\hat{G}^{A}$ and $\hat{G}^{K}$ must written in particle-hole space ($\hat{G}$ notation) to account for the pairing interaction of superconductors.

The lesser and greater Green's functions for superconductors are then given by

$$\hat{G}^{>}(1,1') = -i\hat{\tau}_z \begin{bmatrix} \left\langle \psi_\uparrow(1)\,\psi_\uparrow^\dagger(1') \right\rangle & \left\langle \psi_\uparrow(1)\,\psi_\downarrow(1') \right\rangle \\ \left\langle \psi_\downarrow^\dagger(1)\,\psi_\uparrow^\dagger(1') \right\rangle & \left\langle \psi_\downarrow^\dagger(1)\,\psi_\downarrow(1') \right\rangle \end{bmatrix}; \tag{2.17}$$

$$\hat{G}^{<}(1,1') = i\hat{\tau}_z \begin{bmatrix} \left\langle \psi_\uparrow^\dagger(1')\,\psi_\uparrow(1) \right\rangle & \left\langle \psi_\downarrow(1')\,\psi_\uparrow(1) \right\rangle \\ \left\langle \psi_\uparrow^\dagger(1')\,\psi_\downarrow^\dagger(1) \right\rangle & \left\langle \psi_\downarrow(1')\,\psi_\downarrow^\dagger(1) \right\rangle \end{bmatrix}. \tag{2.18}$$

The diagonal elements are the standards Fermionic Green's functions, while the off-diagonal elements take care of the effect of Cooper pairing. These last components have a non-zero expectation value because the BCS ground state does not conserve the number of particles. A useful approximation can be made to simplify the calculation of the properties of structured superconducting nanodevices. Assuming the the interesting physics of transport in Josephson junctions is determined by a thin band of states near the Fermi surface, we introduce the quasiclassical approximation in the next subsection.

2.1.2 Quasiclassical Superconductivity

The Green's function is known to oscillate in the relative coordinates $|\mathbf{r}_1 - \mathbf{r}_2|$ roughly at the Fermi wavelength $\frac{2\pi}{p_F}$ [15]. These oscillations are much shorter than the coherence length $\frac{v_F}{\Delta}$ of the superconductors used in typical nanocircuits. In problems involving the proximity effect or Andreev reflections, we can ignore the information from fast oscillations by integrating out the relative coordinates dependence since the physics of transport in Josephson junction depend on the ratio $\frac{\Delta}{E_F}$ which is always small[16]. Indeed, after doing a spatial Fourier transform, we find the Green's function is highly peaked at $|\mathbf{p}| = p_F$. However it is important to keep its dependence on the direction of p_F for transport problems. The quasiclassical approximation then involves keeping only the terms proportional to the first order spatial derivatives in the equation defining the Green's function. If we define $\xi = \frac{p^2}{2m} - \mu$, the quasiclassical Green's function can be written [17] as

$$\check{g}(\mathbf{r}, \mathbf{v}_F, E) \equiv \frac{i}{\pi} \int d\xi \check{G}(\xi, \mathbf{v}_F, \mathbf{r}, E). \tag{2.19}$$

2.2 Transport Through a Ballistic Quantum Point Contact

2.2.1 The Model

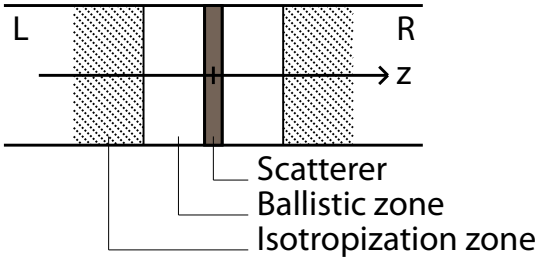

Figure 2.5: A channel is divided in three zones to account for the boundary conditions on both sides of the scatterer and in the terminals[18].

As shown in figure 2.5, a conduction channel is modelled as a device with two terminals such that their Green's function is static and given by $\check{G}^L$ on the left and $\check{G}^R$ on the right. A ballistic region contains a scatterer with potential $U(z)$ whose dimensions are assumed to be much small than the Fermi wavelength and the mean free path of the electrons and holes[10]. In this region it is assumed that the kinetic energy of the particles is conserved such that we can describe the transport of electrons using a transfer matrix without any loss. Finally an isotropization zone is used to describe the relaxation process by which the Green's function in the ballistic zone is conditioned to relax to its value in the terminals. This can occur through scattering with phonons or impurities and this is where the self-energy picks up an imaginary part.

In one dimension, the Gor'kov equation defining the Keldysh Green's function $\check{G}$ is [19]

$$\left(i\check{\tau}_z\frac{\partial}{\partial t}+\frac{1}{2m}\frac{\partial^2}{\partial z^2}+\check{\Delta}-\Phi-U-\check{\Sigma}+\mu\right)\check{G}(z,z';t,t')=\check{1}\delta(z-z')\,\delta(t-t') \qquad (2.20)$$

as well as its conjugate. The Nambu-Keldysh Green's function has the form $\check{G}=\begin{pmatrix}\hat{G}^R & \hat{G}^K\\ \hat{0} & \hat{G}^A\end{pmatrix}$ and the self-energy can be written as $\check{\Sigma}=\begin{pmatrix}\hat{\Sigma}^R & \hat{\Sigma}^K\\ \hat{0} & \hat{\Sigma}^A\end{pmatrix}$. The product denotes a convolu-

tion in the internal time argument

$$\check{\Sigma}\check{G} = \int dt_1 \check{\Sigma}\left(t, t_1\right) \check{G}\left(t_1, t'\right). \tag{2.21}$$

The potential $U\left(z\right)$ is such that

$$\epsilon_{FL} + U\left(z < -\delta\right) = \epsilon_{FR} + U\left(z > \delta\right) = \mu \tag{2.22}$$

and the chemical potential μ remains constant through the system. Also, a matrix $\check{\tau}_z = \begin{pmatrix} \hat{\tau}_z & \hat{0} \\ \hat{0} & \hat{\tau}_z \end{pmatrix}$ is defined and the pairing matrix takes the form

$$\check{\Delta} = \begin{pmatrix} \hat{\Delta} & \hat{0} \\ \hat{0} & \hat{\Delta} \end{pmatrix} \quad \hat{\Delta} = \begin{pmatrix} 0 & \Delta \\ -\Delta^* & 0 \end{pmatrix}. \tag{2.23}$$

If we suppose that the Fermi energy is the same on both side $\epsilon_F = \epsilon_{FL} = \epsilon_{FR}$, then condition 2.22 allows to rewrite equation 2.20 as

$$\left(\frac{1}{2m}\frac{\partial^2}{\partial z^2} + \epsilon_F + i\check{\tau}_z\frac{\partial}{\partial t} + \check{\Delta} - \Phi - \check{\Sigma}\right)\check{G}\left(z, z'; t, t'\right) = \check{1}\delta\left(z - z'\right)\delta\left(t - t'\right). \tag{2.24}$$

2.2.2 Quasiclassical Approximation

We want to obtain a function $\check{G}\left(z, z'\right)$ which is continuous at $z = z'$ and can be evaluated at any point of the channel. We can expand the Green's function as

$$\check{G}\left(z, z'\right) = \sum_{p_z, p'_z} e^{ip_z z - ip'_z z'}\check{G}_{p_z p'_z} \tag{2.25}$$

It is strongly peaked around $|p_z| = p_F$, to take this into account we can replace p_z by p_F and represent the quasiclassical function as

$$\check{G}\left(z, z'\right) = \sum_{\sigma, \sigma' = \pm 1} e^{ip_F(\sigma z - \sigma' z')}\check{G}_{\sigma\sigma'} \tag{2.26}$$

where σ and σ' are the directions of propagation. The functions $\check{G}_{\sigma\sigma'}$ have the property that $\frac{\partial^2}{\partial z^2}\check{G}_{\sigma\sigma'}\left(z, z'\right) \approx 0$. Using this property, we can show that

$$\left(\frac{1}{2m}\frac{\partial^2}{\partial z^2} + \epsilon_F\right)\check{G}\left(z, z'\right) = \sum_{\sigma, \sigma' = \pm 1} e^{ip_F(\sigma z - \sigma' z')} i\sigma v_F \frac{\partial}{\partial z}\check{G}_{\sigma\sigma'}\left(z, z'\right) \tag{2.27}$$

In the case $z \neq z'$, the Dirac delta $\delta(z - z')$ of equation 2.24 becomes zero and each component of the left-hand side becomes

$$\left(i\sigma v_F \frac{\partial}{\partial z} + i\check{\tau}_z \frac{\partial}{\partial t} + \check{\Delta} - \Phi - \check{\Sigma}\right) \check{G}_{\sigma\sigma'}(z, z') = \check{0}. \tag{2.28}$$

We can get the conjugate equation in a similar way

$$\check{G}_{\sigma\sigma'}(z, z') \left(-i\sigma' v_F \frac{\partial}{\partial z'} - i\check{\tau}_z \frac{\partial}{\partial t'} + \check{\Delta} - \Phi - \check{\Sigma}\right) = \check{0}. \tag{2.29}$$

To match the functions $\check{G}_{\sigma\sigma'}(z, z')$ at $z = z'$, we impose the continuity condition

$$\check{G}(z + 0, z) = \check{G}(z - 0, z) \tag{2.30}$$

and find the jump in the spatial derivative by integrating equation 2.24 from $z = z' - 0$ to $z = z' + 0$ such that

$$\left[\frac{\partial}{\partial z}\check{G}(z, z')\right]_{z=z'-0}^{z=z'+0} = 2m\check{1}\delta(t - t'). \tag{2.31}$$

By replacing 2.26 into 2.30 and 2.31, we get the continuity condition of the $\check{G}_{\sigma\sigma'}$

$$\check{G}_{\sigma\sigma'}(z + 0, z) - \check{G}_{\sigma\sigma'}(z - 0, z) = -\frac{i\sigma}{v_F}\check{1}\delta_{\sigma\sigma'}\delta(t - t'). \tag{2.32}$$

This condition is satisfied if we define the components as

$$\check{G}_{\sigma\sigma'}(z, z'; t, t') = -\frac{i}{2v_F}\left[\check{g}_{\sigma\sigma'}(z, z'; t, t') + \sigma\delta_{\sigma\sigma'}\delta(t - t')\,\mathrm{sign}\,(\mathrm{z} - \mathrm{z}')\right] \tag{2.33}$$

where the functions $\check{g}_{\sigma\sigma'}$ are continuous at $z = z'$.

We go in the center-of-mass frame $\bar{z} = \frac{z+z'}{2}$ and $\Delta z = z - z'$[20]. This allows us to define two new functions where the fast oscillation in Δz has been integrated out. In the case $\sigma = \sigma'$ we get

$$\check{g} \equiv \check{g}_\sigma(\bar{z}; t, t') = \sum_{\sigma'} \int d(\Delta z)\, e^{i\sigma' p_F \Delta z} \delta_{\sigma\sigma'} \check{G}_{\sigma\sigma'}\left(\bar{z} + \frac{\Delta z}{2}, \bar{z} - \frac{\Delta z}{2}; t, t'\right). \tag{2.34}$$

In the case $\sigma = -\sigma'$, we find

$$\check{\mathcal{G}} \equiv \check{\mathcal{G}}_\sigma(\bar{z}; t, t') = \sum_{\sigma'} \int d(\Delta z)\, e^{i\sigma' p_F \Delta z} \left[1 - \delta_{\sigma\sigma'}\right] \check{G}_{\sigma\sigma'}\left(\bar{z} + \frac{\Delta z}{2}, \bar{z} - \frac{\Delta z}{2}; t, t'\right). \tag{2.35}$$

If we integrate equations 2.28 and 2.29 with the operator $\sum_{\sigma'} \int d(\Delta z)\, e^{i\sigma' p_F \Delta z} \delta_{\sigma\sigma'}$ and subtract them then we get the quasiclassical equation for $\check{g}$:

$$\sigma v_F \frac{\partial}{\partial \bar{z}} \check{g} + \check{\tau}_z \frac{\partial}{\partial t} \check{g} + \frac{\partial}{\partial t'} \check{g} \check{\tau}_z + \check{H}(t)\, \check{g} - \check{g} \check{H}(t') + i \left(\check{\Sigma} \check{g}\right)(t,t') - i \left(\check{g} \check{\Sigma}\right)(t,t') = \check{0}. \quad (2.36)$$

Here $i\check{H}(t) = \check{\Delta}(t) - \Phi(t)$. In the same way, if we integrate equations 2.28 and 2.29 with the operator $\sum_{\sigma'} \int d(\Delta z)\, e^{i\sigma' p_F \Delta z} [1 - \delta_{\sigma\sigma'}]$ and add them then we get the quasiclassical equation for $\check{\mathcal{G}}$[19]:

$$\sigma v_F \frac{\partial}{\partial \bar{z}} \check{\mathcal{G}} + \check{\tau}_z \frac{\partial}{\partial t} \check{\mathcal{G}} - \frac{\partial}{\partial t'} \check{\mathcal{G}} \check{\tau}_z + \check{H}(t)\, \check{\mathcal{G}} + \check{\mathcal{G}} \check{H}(t') + i \left(\check{\Sigma} \check{\mathcal{G}}\right)(t,t') + i \left(\check{\mathcal{G}} \check{\Sigma}\right)(t,t') = \check{0}. \quad (2.37)$$

2.2.3 Boundary Condition from the Scatterer

Now we take care of the boundary condition at the scattering interface. It is assumed that the barrier potential $U(z)$ varies smoothly compared to the interatomic distance such that the scattering formalism can be used. The transfer matrix $\bar{M}$ relates the wavefunctions on the right ($\psi_\sigma^R \equiv \psi_\sigma(\bar{z} > 0)$) to the wavefunctions on the left ($\psi_\sigma^L \equiv \psi_\sigma(\bar{z} < 0)$) such that

$$\psi_\sigma^L = \sum_{\sigma'} \bar{M}_{\sigma\sigma'} \psi_{\sigma'}^R \quad (2.38)$$

The Green's functions $\check{G}_{\sigma\sigma'}$ transform as a product of wavefunctions such that

$$\check{G}_{\sigma\sigma'}^L = \sum_{\sigma'',\sigma'''} \left(\bar{M}^\dagger\right)_{\sigma'\sigma'''} \check{G}_{\sigma'''\sigma''}^R \bar{M}_{\sigma''\sigma'} \quad (2.39)$$

If we plug back equation 2.33 into 2.39 we get

$$\check{g}_{\sigma\sigma'}^L = \sum_{\sigma'',\sigma'''} \left(\bar{M}^\dagger\right)_{\sigma'\sigma'''} \check{g}_{\sigma'''\sigma''}^R \bar{M}_{\sigma''\sigma'} \quad (2.40)$$

The bar notation was introduced $\bar{A} \equiv \left\{\check{A}_{\sigma\sigma'}\right\}$ for matrices whose elements are the Keldysh matrices over the different directions σ and σ'. Some important properties of the transfer matrix will be used. If the matrix $\bar{\Sigma}_{\sigma\sigma'}^z \equiv \sigma \delta_{\sigma\sigma'}$ is defined, conservation of probability imposes a pseudo-unitarity condition for the transfer matrix

$$\bar{M} \bar{\Sigma}^z \bar{M}^\dagger = \bar{\Sigma}^z. \quad (2.41)$$

The transmission eigenvalues of $\bar{M}$ will be extracted using the self-adjoint matrix $\bar{Q} = \bar{M}^\dagger \bar{M}$ and its inverse $\bar{Q}^{-1} = \bar{\Sigma}^z \bar{Q} \bar{\Sigma}^z$, which have the same set of inverse pairs of eigenvalues.

Let's make the boundary condition 2.40 more meaningful. We introduce quasiclassical Green's functions symmetrical and antisymmetrical in direction space such that $\check{g}_\sigma(\bar{z}) = \check{g}_s(\bar{z}) + \sigma \check{g}_a(\bar{z})$ and $\check{\mathcal{G}}_\sigma(\bar{z}) = \check{\mathcal{G}}_s(\bar{z}) + \sigma \check{\mathcal{G}}_a(\bar{z})$. The antisymmetric Green's function is

$$\check{g}_a(\bar{z}) = \frac{1}{2} \sum_{\sigma=1,-1} \sigma \delta_{\sigma\sigma'} \check{g}_\sigma(\bar{z}) = \frac{1}{2} \mathrm{Tr}_\sigma \left[\bar{\Sigma}^{\mathrm{z}} \bar{\mathrm{g}}(\bar{\mathrm{z}}) \right] \tag{2.42}$$

where $\mathrm{Tr}_\sigma \left(\bar{\mathrm{G}} \right) = \sum_{\sigma=1,-1} \check{\mathrm{G}}_{\sigma\sigma}$ and in the same way,

$$\check{g}_s(\bar{z}) = \frac{1}{2} \mathrm{Tr}_\sigma \left[\bar{\mathrm{g}}(\bar{\mathrm{z}}) \right]. \tag{2.43}$$

For the reflection Green's functions $\check{\mathcal{G}}_\sigma$, we introduce a matrix $\bar{\Sigma}^x$ such that $\bar{\Sigma}^x_{\sigma\sigma'} = 1 - \delta_{\sigma\sigma'}$ is 1 if $\sigma \neq \sigma'$ and 0 if $\sigma = \sigma'$. Then we have

$$\check{\mathcal{G}}_a(\bar{z}) = \frac{1}{2} \mathrm{Tr}_\sigma \left[\bar{\Sigma}^{\mathrm{z}} \bar{\mathrm{g}}(\bar{\mathrm{z}}) \bar{\Sigma}^{\mathrm{x}} \right] \tag{2.44}$$

and

$$\check{\mathcal{G}}_s(\bar{z}) = \frac{1}{2} \mathrm{Tr}_\sigma \left[\bar{\mathrm{g}}(\bar{\mathrm{z}}) \bar{\Sigma}^{\mathrm{x}} \right] \tag{2.45}$$

Using $2 + MM^\dagger + \left(MM^\dagger\right)^{-1} = \frac{1}{4} \begin{pmatrix} tt^\dagger & 0 \\ 0 & t'^\dagger t' \end{pmatrix}$, as well as the cyclical property of the trace and the properties of the transfer matrix we get the set of four conditions imposed by the scattering interface

$$\begin{array}{rcl} \check{g}_a^R & = & \check{g}_a^L \equiv \check{g}_a \\ \check{\mathcal{G}}_a^R & = & \check{\mathcal{G}}_a^L \equiv \check{\mathcal{G}}_a \\ \check{g}_s^R - \check{g}_s^L & = & -\sqrt{R} \left(\check{\mathcal{G}}_s^R + \check{\mathcal{G}}_s^L \right) \\ \sqrt{R} \left(\check{g}_s^R + \check{g}_s^L \right) & = & \check{\mathcal{G}}_s^L - \check{\mathcal{G}}_s^R \end{array} \tag{2.46}$$

where $R = 1 - D$.

2.2.4 Isotropization

Far from the boundary ($\bar{z} \gg l$), the current and the particle density can be expressed in terms of the standard quasiclassical Green's function $\check{g}_\sigma(\bar{z})$. Let us express the boundary

condition as functions of $\check{g}_\sigma(\bar{z})$. Indeed, it is possible to establish the following relations [19]:

$$\check{g}_\sigma \check{\mathcal{G}}_\sigma = \text{sign}(\bar{z})\,\sigma\check{\mathcal{G}}_\sigma \tag{2.47}$$

$$\check{g}_\sigma^2 = \check{1}\delta(t-t') = \check{\mathbf{1}} \tag{2.48}$$

From these we can show that $\{\check{g}_s, \check{g}_a\} = \check{0}$ and $(\check{g}_s)^2 + (\check{g}_a)^2 = \check{\mathbf{1}}$. From there, we define $\check{g}_s^\pm = \frac{1}{2}\left(\check{g}_s^R \pm \check{g}_s^L\right)$ for which we can show that $\{\check{g}_s^+, \check{g}_s^-\} = \check{0}$ and $\{\check{g}_s^\pm, \check{g}_a\} = \check{0}$. The boundary conditions 2.46 can be rewritten using only $\check{g}_\sigma$'s [19]:

$$\check{g}_a\left[R\left(\check{g}_s^+\right)^2 + \left(\check{g}_s^-\right)^2\right] = D\check{g}_s^-\check{g}_s^+ \tag{2.49}$$

The solution to equation 2.36 can be written in the form [21]

$$\check{g}_\sigma(\bar{z}) = e^{-\check{K}(\bar{z})\frac{\bar{z}}{v_F}}\check{C}_\sigma(\bar{z})\,e^{\check{K}(\bar{z})\frac{\bar{z}}{v_F}} + \check{G}_{\text{Bulk}}(\bar{z}) \tag{2.50}$$

where $v_F\frac{\partial}{\partial\bar{z}}\check{C}_\sigma(z) = \check{0}$. Using 2.46, we get $\check{C}_a^L = \check{C}_a^R \equiv \check{C}_a$ where $\check{C}_a(\bar{z}) = \frac{1}{2}\sum_\sigma \sigma\check{C}_\sigma(\bar{z})$. To make sure that $\lim_{\bar{z}\to\pm\infty}\check{g}_\sigma(\bar{z}) = \check{G}_{\text{Bulk}}^{R/L}$, we get the conditions

$$\begin{array}{c}\check{g}_\sigma(\bar{z})\,\check{C}_\sigma(\bar{z}) = -\text{sign}(\bar{z})\,\sigma\check{C}_\sigma(\bar{z}) \\ \check{C}_\sigma(\bar{z})\,\check{g}_\sigma(\bar{z}) = \text{sign}(\bar{z})\,\sigma\check{C}_\sigma(\bar{z})\end{array} \tag{2.51}$$

We define $\check{G}_{\text{Bulk}}^\pm = \frac{1}{2}\left(\check{G}_{\text{Bulk}}^R \pm \check{G}_{\text{Bulk}}^L\right)$. These relations imply that $\check{g}_s^+ = \check{G}_{\text{Bulk}}^+ + \check{G}_{\text{Bulk}}^-\check{C}_a$ and $\check{g}_s^- = \check{G}_{\text{Bulk}}^+\check{C}_a + \check{G}_{\text{Bulk}}^-$. We have $\left\{\check{G}_{\text{Bulk}}^\pm, \check{C}_a\right\} = \check{0}$ and $\left(\check{G}_{\text{Bulk}}^+\right)^2 + \left(\check{G}_{\text{Bulk}}^-\right)^2 = \check{\mathbf{1}}$. From this we can show using 2.49 that

$$\check{g}_a = D\check{G}_{\text{Bulk}}^-\check{G}_{\text{Bulk}}^+\check{N}^{-1} \tag{2.52}$$

where $\check{N} = \check{1} - D\left(\check{G}_{\text{Bulk}}^-\right)^2$. After some algebra we get

$$\check{g}_s^R = D\left(\check{G}_{\text{Bulk}}^+ + R\check{G}_{\text{Bulk}}^-\right)\check{N}^{-1} \tag{2.53}$$

Finally, using 2.47, we get [22]

$$\check{\mathcal{G}}_a = -\sqrt{R}\check{N}^{-1} \tag{2.54}$$

$$\check{\mathcal{G}}_s^R = -\sqrt{R}\check{G}_{\text{Bulk}}^R\check{N}^{-1} \tag{2.55}$$

2.2.5 Bulk Solutions

Let's note that the bulk solution to the quasiclassical equations are given by [19]

$$\check{g}_j\left(t,t'\right)=\check{S}_j\left(t\right)\check{g}\left(t-t'\right)\check{S}_j^{\dagger}\left(t'\right) \tag{2.56}$$

where $\check{g}\left(t\right)=\int\check{g}\left(\epsilon\right)e^{-i\epsilon t}\frac{d\epsilon}{2\pi}$ and the matrices

$$\check{S}_j=\begin{pmatrix}\hat{S}_j & \hat{0}\\ \hat{0} & \hat{S}_j\end{pmatrix}\quad\hat{S}_j=\begin{pmatrix}e^{i\frac{\phi_j}{2}} & 0\\ 0 & e^{-i\frac{\phi_j}{2}}\end{pmatrix}. \tag{2.57}$$

The retarded and advanced Green's functions take the form

$$\hat{g}^{R(A)}=g^{R(A)}\hat{\tau}_z+f^{R(A)}i\hat{\tau}_y \tag{2.58}$$

where

$$g^{R(A)}=\left(\frac{\epsilon}{\Delta}\right)f^{R(A)}=\frac{\epsilon}{\sqrt{\left(\epsilon\pm i\gamma\right)^2-\Delta^2}}. \tag{2.59}$$

In the energy representation, the homogeneous Green's function take the form

$$\check{g}\left(\epsilon\right)=\begin{pmatrix}\hat{g}^R\left(\epsilon\right) & \left[\hat{g}^R\left(\epsilon\right)-\hat{g}^A\left(\epsilon\right)\right]\tanh\left(\frac{\epsilon}{2\mathrm{T}}\right)\\ \hat{0} & \hat{g}^A\left(\epsilon\right)\end{pmatrix}. \tag{2.60}$$

2.2.6 Computing Observables

We can extract the bound state energy by setting $\check{N}=\check{0}$ and we find

$$E_{J\pm}=\pm\Delta\sqrt{1-D\sin^2\left(\frac{\phi}{2}\right)}. \tag{2.61}$$

These energies are plotted in figure 2.6, where it can be seen that the pair of levels is pinned at the Fermi surface when $D=1$ and $\phi=\pi$. When we change the phase, the degeneracy of the bound states is lifted and the level gets closer to the gap. At $D=0$ or $\phi=0$, the bound state energy becomes pinned to the gap energy. The density of states can be computed from

$$N\left(\epsilon\right)=\frac{N_0}{4}\mathrm{Tr}\left(\hat{\mathrm{g}}_{\mathrm{s}}^{\mathrm{K}}\right). \tag{2.62}$$

The noise at a given frequency moves a particle from an occupied state at energy ϵ to an

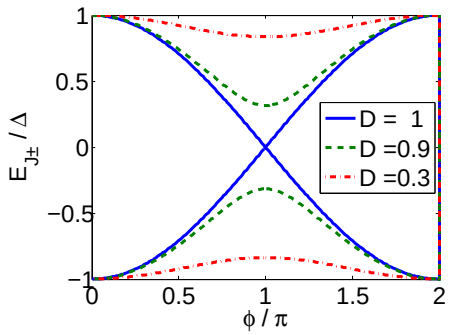

Figure 2.6: Bound state energy as a function of phase ϕ for different transparencies D.

empty state with energy $\epsilon \pm \omega$. As seen in figure 2.7, the density of states depends on the phase difference and the transmission eigenvalue across the channel while the temperature determine the occupancy of those states. At temperature $T \ll \Delta$, there can be four possible processes for the generation of noise. First there can be low-frequency transitions within a bound state with non-zero linewidth. A second type of transitions between bound states can also occur for $\omega < \Delta$. Furthermore, there can be transitions between a bound state to the continuum of states ($\epsilon > \Delta$). Finally we should observe transitions from one continuum to the other when $\omega > 2\Delta$.

If one was interested in computing the current in the junction, the first quantity to evaluate [18] would be the matrix current

$$\langle \check{I} \rangle = \frac{2e^2}{\pi} \check{g}_a. \tag{2.63}$$

However, we note that the matrix current does not contains enough information to compute the noise, which is treated in the next section. The electrical current could be computed from this quantity using

$$\langle I \rangle = \frac{1}{4e} \int d\epsilon \mathrm{Tr} \left(\hat{\tau}_z \hat{\mathrm{I}}^{\mathrm{K}} \right) \tag{2.64}$$

where $\hat{I}^K$ is the Keldysh component of $\check{I}$. This last formula would be sufficient to recover the first Josephson relations as well as the Ambegaokar-Baratoff formula in the limit of small D. Let's finally note that the frequency and phase-dependent Fano factor, which is

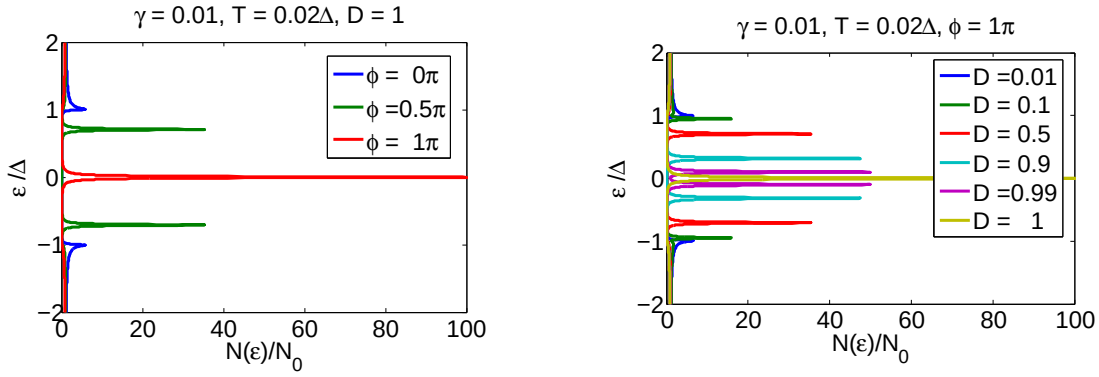

Figure 2.7: (Left) Density of states as a function of phase for a perfectly transmitting channel. (Right) Density of states for different transparencies when $\phi = \pi$.

the ratio of the variance over the average current, is given by

$$F = \frac{S_I(\omega, \phi)}{\langle I(\phi) \rangle}. \tag{2.65}$$

2.3 Supercurrent Noise

The symmetrized current-current correlation function is defined [22] as

$$\begin{array}{rcl} K_I(t_1,t_2) & = & \frac{1}{2}\langle \delta I(t_1)\,\delta I(t_2)+\delta I(t_2)\,\delta I(t_1)\rangle \\ & = & \frac{1}{2}\langle I(t_1)\,I(t_2)+I(t_2)\,I(t_1)\rangle - \langle I(t_1)\rangle\langle I(t_2)\rangle \end{array} \tag{2.66}$$

where $I(t)$ is the time-dependant current operator in the Heisenberg picture. The time arguments $t_{1,2}$ follow the real time Keldysh contour from $t=-\infty$ to $t=\infty$ then back again. For a channel of area A, the current density operator is given by

$$\mathbf{j}(\mathbf{r}) = -\frac{ie\hbar}{2m}\left[\hat{\psi}^\dagger(\mathbf{r})\,\nabla\hat{\psi}(\mathbf{r}) - \left(\nabla\hat{\psi}^\dagger(\mathbf{r})\right)\hat{\psi}(\mathbf{r})\right]. \tag{2.67}$$

The field operators are meant to be interpreted as Nambu fields.

In 1D, we plug 2.67 into 2.66 and expand in electron creation and annihilation operators. Then we use Wick's theorem and the definition of the Nambu-Keldysh Green's function to rewrite the current-current correlation function as

$$K_I(t_1,t_2) = -\frac{e^2}{8}\left[\partial_{z_1}-\partial_{z_1'}\right]\left[\partial_{z_2}-\partial_{z_2'}\right]\mathrm{Tr}\left\{\begin{array}{c} \hat{G}^{>}(1',2)\,\hat{\tau}_z\hat{G}^{<}(2',1)\,\hat{\tau}_z \\ +\hat{G}^{<}(1',2)\,\hat{\tau}_z\hat{G}^{>}(2',1)\,\hat{\tau}_z \end{array}\right\}_{\mathrm{z}_1=\mathrm{z}_1'=\mathrm{z}_2=\mathrm{z}_2'=0}. \tag{2.68}$$

We then go in the Fourier representation of the quasiclassical function $\check{g}(1,1')$ and reflections function $\check{\mathcal{G}}(1,1')$. The terms that do not cancel are such that the current-current correlation function becomes

$$K_I(t_1,t_2) = -\frac{e^2p_F^2}{16\pi}\int d^2\rho\sum_{\sigma=\pm1}\mathrm{Tr}\left\{\begin{array}{c} \hat{g}_\sigma^{>}(t_1,t_2)\,\hat{\tau}_z\hat{g}_\sigma^{<}(t_2,t_1)\,\hat{\tau}_z+\hat{g}_\sigma^{<}(t_1,t_2)\,\hat{\tau}_z\hat{g}_\sigma^{>}(t_2,t_1)\,\hat{\tau}_z \\ -\hat{\mathcal{G}}_\sigma^{>}(t_1,t_2)\,\hat{\tau}_z\hat{\mathcal{G}}_{-\sigma}^{<}(t_2,t_1)\,\hat{\tau}_z-\hat{\mathcal{G}}_\sigma^{<}(t_1,t_2)\,\hat{\tau}_z\hat{\mathcal{G}}_{-\sigma}^{>}(t_2,t_1)\,\hat{\tau}_z \end{array}\right\}. \tag{2.69}$$

We then represent these Green's function by their symmetric and antisymmetric components for which we already know the full form. From [22], we get the full form of the two-point current-current correlation function.

$$K_I(t_1,t_2) = -\frac{e^2p_F^2}{8\pi}\int d^2\rho\mathrm{Tr}\left\{\begin{array}{ccc} \hat{g}_s^{>}(t_1,t_2)\,\hat{\tau}_z\hat{g}_s^{<}(t_2,t_1)\,\hat{\tau}_z & + & \hat{g}_s^{<}(t_1,t_2)\,\hat{\tau}_z\hat{g}_s^{>}(t_2,t_1)\,\hat{\tau}_z \\ + \hat{g}_a^{>}(t_1,t_2)\,\hat{\tau}_z\hat{g}_a^{<}(t_2,t_1)\,\hat{\tau}_z & + & \hat{g}_a^{<}(t_1,t_2)\,\hat{\tau}_z\hat{g}_a^{>}(t_2,t_1)\,\hat{\tau}_z \\ - \hat{\mathcal{G}}_s^{>}(t_1,t_2)\,\hat{\tau}_z\hat{\mathcal{G}}_s^{<}(t_2,t_1)\,\hat{\tau}_z & - & \hat{\mathcal{G}}_s^{<}(t_1,t_2)\,\hat{\tau}_z\hat{\mathcal{G}}_s^{>}(t_2,t_1)\,\hat{\tau}_z \\ + \hat{\mathcal{G}}_a^{>}(t_1,t_2)\,\hat{\tau}_z\hat{\mathcal{G}}_a^{<}(t_2,t_1)\,\hat{\tau}_z & + & \hat{\mathcal{G}}_a^{<}(t_1,t_2)\,\hat{\tau}_z\hat{\mathcal{G}}_a^{>}(t_2,t_1)\,\hat{\tau}_z \end{array}\right\} \tag{2.70}$$

We finally Fourier transform the time coordinates and get the final noise expression of a channel to evaluate. From [5]

$$\begin{aligned} S_I(\omega) &= \tfrac{1}{2\pi}\int d\tau e^{-i\omega\tau} K(\tau) \\ &= \tfrac{e^2}{32\pi^2\hbar}\textstyle\sum_{\pm\omega,\pm}\int d\epsilon \mathrm{Tr}\begin{bmatrix} & \hat{g}_s^{>}(\epsilon)\hat{\tau}_z\hat{g}_s^{<}(\epsilon\pm\omega)\hat{\tau}_z & + & \hat{g}_s^{<}(\epsilon)\hat{\tau}_z\hat{g}_s^{>}(\epsilon\pm\omega)\hat{\tau}_z \\ + & \hat{g}_a^{>}(\epsilon)\hat{\tau}_z\hat{g}_a^{<}(\epsilon\pm\omega)\hat{\tau}_z & + & \hat{g}_a^{<}(\epsilon)\hat{\tau}_z\hat{g}_a^{>}(\epsilon\pm\omega)\hat{\tau}_z \\ - & \hat{\mathcal{G}}_s^{>}(\epsilon)\hat{\tau}_z\hat{\mathcal{G}}_s^{<}(\epsilon\pm\omega)\hat{\tau}_z & - & \hat{\mathcal{G}}_s^{<}(\epsilon)\hat{\tau}_z\hat{\mathcal{G}}_s^{>}(\epsilon\pm\omega)\hat{\tau}_z \\ + & \hat{\mathcal{G}}_a^{>}(\epsilon)\hat{\tau}_z\hat{\mathcal{G}}_a^{<}(\epsilon\pm\omega)\hat{\tau}_z & + & \hat{\mathcal{G}}_a^{<}(\epsilon)\hat{\tau}_z\hat{\mathcal{G}}_a^{>}(\epsilon\pm\omega)\hat{\tau}_z \end{bmatrix}. \end{aligned} \tag{2.71}$$

We finally have all the required equations to compute the noise as a function of the parameters ω,T,γ,D and ϕ. Considering that the superconducting gap of Al is about 9 Ghz and that superconducting qubits are operated near 50 mK, we estimate that the temperature $T/\Delta \approx 0.1$. While unknown, it makes sense that the relaxation rate $\gamma/\Delta \ll 1$.

The expression for the frequency dependent noise can hardly be evaluated analytically, the convolution is done numerically over an energy range and a coarse-graining such that the numerical error drops to less than 1%. Also, the spectra are shown in the range $-3\Delta < \omega < 3\Delta$ to highlight the absorption processes $\omega > 0$ and the emission processes $\omega < 0$. The symmetrized noise as it is measured corresponds to "folding" the spectrum around $\omega = 0$ such that, if $\omega > 0$, $S_I^{\mathrm{symm}}(\omega) = \frac{S_I(\omega)+S_I(-\omega)}{2}$.

The results highlight different aspects of Andreev physics. Near $\omega = 0$, we observe the effect of transitions within the bound state linewidth (or within the continuum if it is thermally occupied). A peak can also occur at low frequencies if the bound state levels are very close to the Fermi level, which is the case for open channels $D \approx 1$. In some case we can also see the effect of transitions between the bound states in the range $\omega < 2\Delta$ as an additional peak in the spectrum when $D < 1$. Furthermore, transitions between the bound state and the continuum can produce two step-like features in the spectrum, one has to be in the range $0 < \omega < \Delta$ and the other in the range $\Delta < \omega < 2\Delta$. Finally, transitions from one continuum to the other appear in the spectrum when $\omega > 2\Delta$ as a linear contribution and correspond to resistive quasi-particle generation. A high-energy cutoff is not provided but it is assumed to exist at frequencies $\omega \gg 2\Delta$.

The noise spectrum for different channel transparencies is shown in figure 2.8 for a phase difference $\phi = \pi$. We observe a strong non-linear relation between the height of the zero-frequency peak and the transmission eigenvalue. Indeed, it can be seen from figure 2.6 that a slight deviation from $D = 1$ leads to lifting the degeneracy of the bound state pinned at the Fermi level. Lowering the transparency separates those level even more such that a second peak can already be seen appearing at $\omega > 0$ when $D = 0.9$.

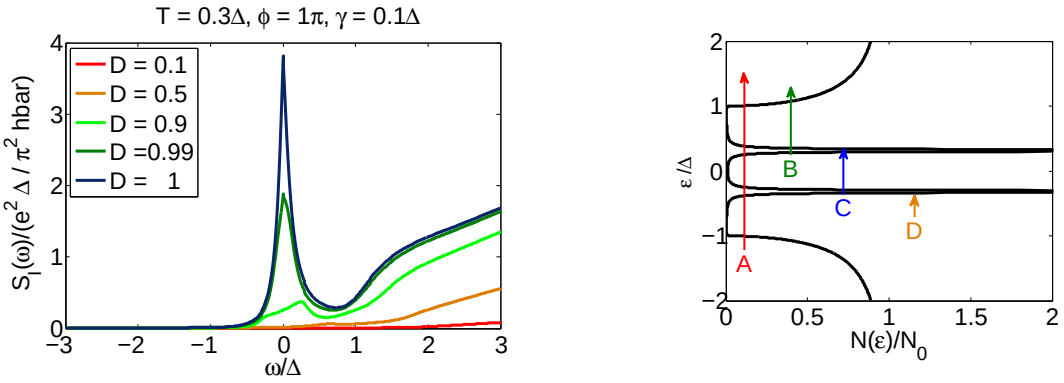

Figure 2.8: (Left) The transparency dependence of the noise spectrum is shown. The case $\phi = \pi$ is the most interesting as the effect of the opening of the bound state can be seen. (Right) The possible transitions contributing to the noise are shown. A are continuum to continuum transitions, B are bound state to continuum transitions, C are subgap transitions and D are transitions within the linewidth of a bound state.

As shown in figure 2.9, the opening of the bound state is well seen if we look at the spectrum at different phases. In the case of a fully open channel, the noise is greater at $\phi = \pi$ where the bound state is pinned to the Fermi level. We also notice the step feature near $\omega = \Delta$ corresponding to transition from the bound state to the continuum. At $\phi = \frac{\pi}{2}$, we notice a small zero-frequency noise contribution coming from transition within the thermally occupied bound state. A second "peak" is visible and correspond to transition from one bound state level to the other. At $\phi = 0$, the small contribution of zero-frequency noise remaining comes from thermally occupied states in the continuum and we can clearly see the appearance of an absorption band around $\omega > 2\Delta$. In the case of an half-open channel, we first observe a strong suppression of the low-frequency noise relative to the fully opened channel case. This is explained by the absence of occupied states near the Fermi level. We can also see that $\phi = \pi$ noise is no longer dominant at $\phi = \pi$ and that the absorption bands $\omega > 2\Delta$ do not have the same amplitude, as a bound state near the Fermi level "steals" spectral weight in the continuum so that the total number of states is unchanged as a function of ϕ.

An analysis of the $\omega = 0$ peak at full transmission and $\phi = \pi$ reveals its Lorentzian character as a function of the relaxation rate γ in figure 2.10. A sharp Lorentzian peak $\gamma \ll 1$ is likely closer to the reality of typical BCS superconductors but each 1/10 factor increase the computation time by a factor 100, which is impractical when a lot of channel

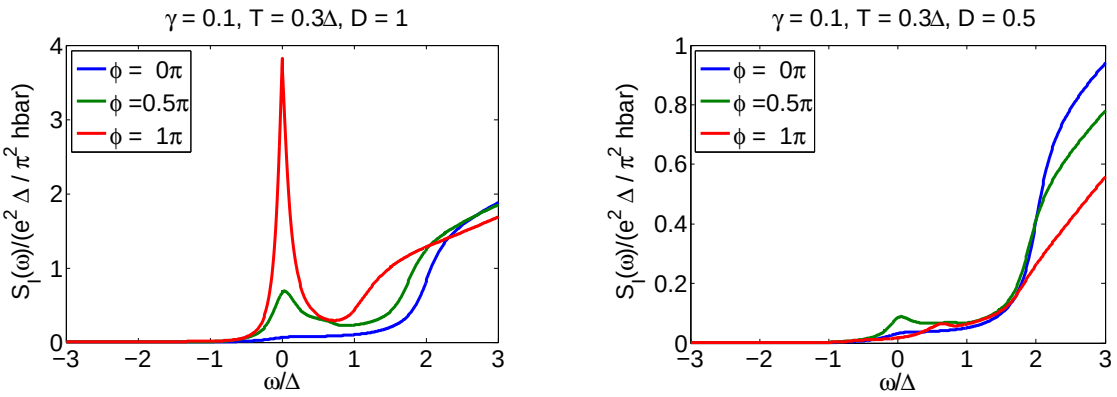

Figure 2.9: Phase dependence of the noise spectrum for pinholes with different transmissions is shown.

are to be considered. Values ranging from 0.01 to 0.3 can be used to extract the physics relevant to the interplay between the temperature and the relaxation rate.

If we take a look at the temperature dependence of the noise spectrum of a fully open channel at $\phi = \pi$ (figure 2.11), we first notice that the height of the zero-frequency peak is constant as long as $T > \gamma$. This implies that the bound state linewidth is fully saturated and its occupation changes only slightly. As the temperature gets lower than the characteristic energy of the relaxation process, the height of the peak diminishes and emission processes are suppressed as the Fermi function is turning in a Heaviside function as $T \to 0$. Since $T < 2\Delta$, the continuum to continuum transitions stay unaffected by temperature change. At $\phi = \frac{\pi}{2}$ where the bound state is somewhere in the middle of the gap, the thermal activation of the bound state to bound state transition becomes obvious as a zero-frequency noise appears when the temperature becomes comparable to the energy splitting inside the gap.

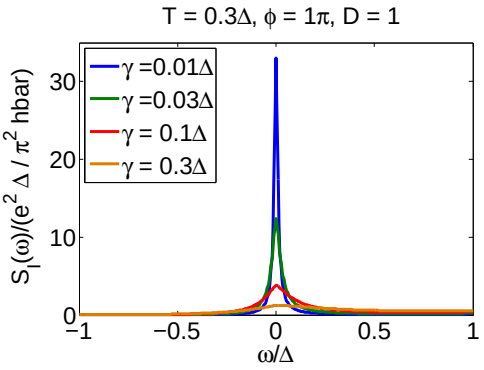

Figure 2.10: The low-frequency noise spectrum as a function of the relaxation rate γ for a fully opened channel is shown. Assuming that γ is a constant over energy, then the peak has a lorentzian shape.

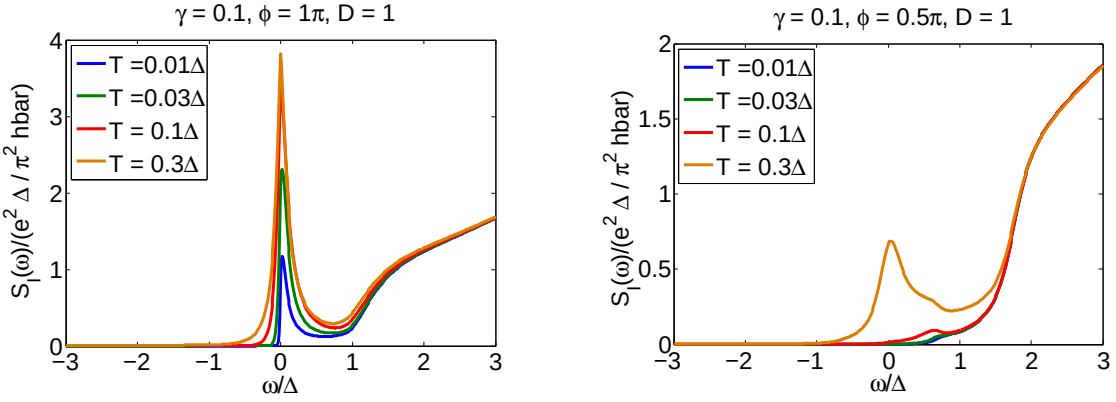

Figure 2.11: Temperature dependence of the noise spectrum for different phases is shown. The left plot corresponds to an opened channel and highlights the diminishing emission processes as T is lowered. The right plot has $D = 0.5$ and shows the activation of transitions between the bound states at high temperature.

Chapter 3

Models of Roughness

This chapter aims to answer the question: what is the noise of a rough Josephson junction? The roughness of a device in the context of quantum transport is modeled as a scattering matrix S over N transverse modes[23]. We assume this scattering matrix is energy independent and its set of transmission eigenvalues $t^{\dagger}t$ form a random set of values D_n. This implies that for a given device, roughness can be modeled as a set of independent channels each with their own D_n as illustrated in figure 3.1. In a large ensemble of similar devices,

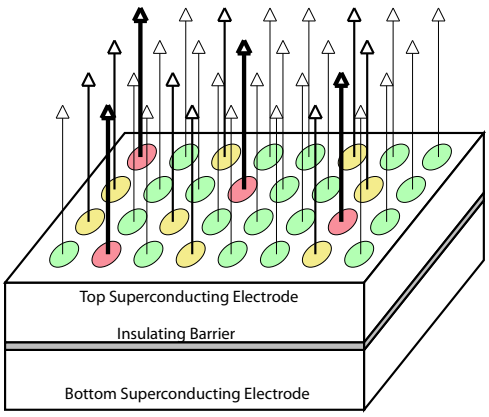

Figure 3.1: Pinhole model.

the distribution of transmission eigenvalues is defined by

$$P(D) \equiv \left\langle \sum_n \delta(D - D_n) \right\rangle \tag{3.1}$$

where $\langle \ldots \rangle$ designates an average over all possible realizations of disorder of a given Hamiltonian. It is normalized such that

$$\int_0^1 dDP(D) = N. \tag{3.2}$$

The distribution function 3.1 is usually obtained by averaging an ensemble of scattering matrices over a random parameter given by the symmetries of the Hamiltonian. Methods and results from random matrix theory are useful to effectuate these computations. Any property $A(D)$ can be averaged over the distribution using

$$\langle A \rangle = \left\langle \sum_n A(D_n) \right\rangle = \int dDA(D) P(D) \tag{3.3}$$

The quantity A is called a linear statistics on the transmission eigenvalues if it does not depend on the product of different eigenvalues. For example, the conductance of a normal metal is given by the Landauer formula $\langle G \rangle = G_0 \langle \sum_n D_n \rangle$, where $G_0 = \frac{2e^2}{h}$. [24] For typical junctions used in nanocircuits, G/G_0 is estimated to range between 250 to 650 in the normal regime[25][26]. However, persistent currents in superconductors are an equilibrium phenomenon whose intensity and direction depend on the phase difference between the two reservoirs as well as the transparency of the barrier between them. If we assume that the scattering zone is much smaller than the coherence length then we can suppose that the phase is constant over each reservoir. Furthermore, we assume there is no phase coherence between the reflections inside the barrier such that there is no Fabry-Perot interference within the device. It means that the transmission eigenvalues used for supercurrent are the same as for normal metals and that we can use the linear statistics method to analyze current and its higher moments in devices which satisfies these conditions.

Since low-frequency noise is an important dephasing mechanism in superconducting qubits, we focus our attention on the noise at zero frequency $S_I(\omega = 0)$. In the following sections, its average and fluctuations from sample to sample are computed for three universal models of disorder. These bimodal distribution are universal in the sense that they do not depend on any microscopic parameters, they only depend on macroscopic conductance. We first look at the behavior of the zero-frequency noise as a function of phase and transparency, especially in the low and high transmission limits where Andreev physics has its most significant effect. We then look at disorder in chaotic cavities, diffusive wires and dirty interfaces, which are common elements of superconducting nanocircuits. A brief description of the derivation of the distribution of transmission eigenvalues for each model is provided. We find out that the average noise is mostly influenced by the physics of partially opened holes which determine a phase ϕ_{max} such that $\langle S_I(\omega = 0, \phi_{max}) \rangle$ is maximal.

However, sample-to-sample fluctuations for disordered devices operating near $\phi = \pi$ are mostly caused by the fluctuation of the likelihood of fully open channels between samples.

3.1 Sample-to-sample Fluctuations

Since nanofabrication techniques are not perfectly reproducible down to the crystal lattice of the deposited material layers, the configuration of defects or impurities producing disorder has to be different in every devices coming out of a wafer. Also, the observed number of pinholes in typical samples is not high enough to average out the effect of its fluctuations on the noise of several samples. Therefore an analysis of the sample-to-sample fluctuations of the noise is required to reveal which parameters affect critically the reproducibility of the noise from one device to another.

Using equation 3.3, we can write the average noise over several samples as

$$\langle S_I(0)\rangle = \int dD S_I(\omega = 0, D)\, P(D). \tag{3.4}$$

Fluctuations of the noise from sample to sample can be computed for a given phase by taking the root mean square of the distribution of noise calculated for each realization of disorder [27]:

$$\delta S_I(0) = \left\langle \left(S_I(0) - \langle S_I(0)\rangle\right)^2 \right\rangle^{\frac{1}{2}}. \tag{3.5}$$

To compute these quantities, we first discretize $P(D)$ into 10000 bins of equal probability with an average D_n for each bin. We then compute the noise contribution of each bin $S_I(\omega = 0, \phi, D_n)$ and generate around 20000 samples from which we can do statistics and find the noise and its fluctuations.

3.2 Tunnel Junction

In this section, we analyze the behavior of the zero-frequency noise $S_I(\omega = 0)$ for the various parameters D, ϕ, γ and T. We also take a closer look at the behavior of the noise for thick tunnel junction ($L \gg \lambda_F$) where all $D_n \ll 1$.

As shown in figure 3.2, we first vary the transparency and the phase. In the neighborhood of $D = 1$ at $\phi = \pi$ we see a rapid increase of the noise as the bound state gets closer to the Fermi energy. Then as we lower the transparency, the $\phi = \pi$ noise is quickly reduced below the noise of the same channel at a different phase. In the middle transparency range the noise scales as $\ln(\mathrm{S_I}(0)) \propto \mathrm{D}$. Then as $D \to 0$, the noise is strongly suppressed. This implies that the noise of a thick tunnel junction without pinholes should be determined by its most transmitting channel. At $\phi = \pi$, the presence of a few pinholes are expected to contribute significantly to the sample-to-sample fluctuations of the noise. From the right plot, it can be seen that for a given phase, the noise is always greater for higher transmission channels. But for a given transparency, $\phi = \pi$ does not usually yield the highest noise, except if $D = 1$. Indeed, for an almost closed channel $D \to 0$, the strongest noise should be obtained near $\phi = 0$. We also remark that since the noise is symmetric around $\phi = \pi$ such that $S_I(\phi) = S_I(2\pi - \phi)$ when $\pi < \phi < 2\pi$ and then 2π-periodic, then the derivative $\left[\frac{\partial}{\partial\phi} S_I(\phi)\right]_{\phi=0,\pi} = 0$.

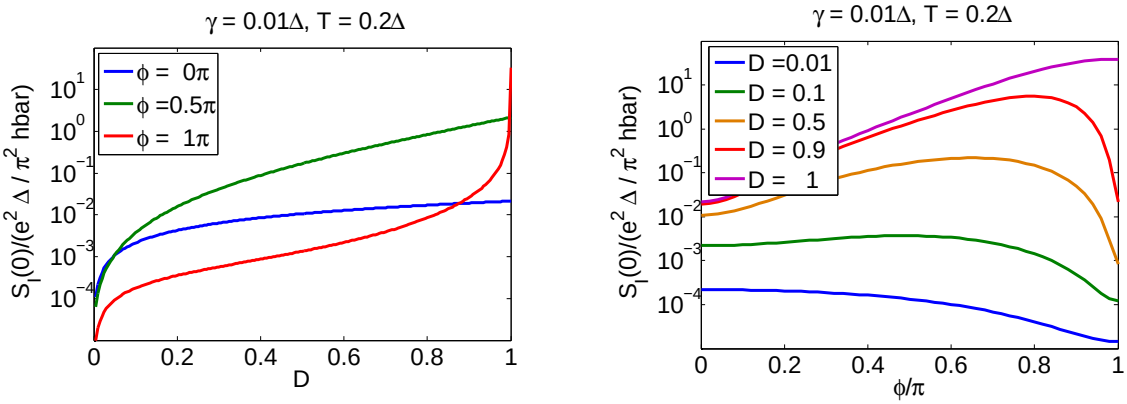

Figure 3.2: The transparency (Left) and phase (Right) dependence of the zero-frequency noise for a single channel are shown.

The temperature dependence of the noise is mainly driven by the thermal activation of the bound state. As can be seen in figure 3.3, the noise of an open pinhole drops significantly

when the temperature gets below the bound state transition energy. Inversely, the noise saturates when the temperature is much greater than the transition energy. In the case of an almost closed channel, the noise becomes very small and temperature independent when $T \ll \Delta$.

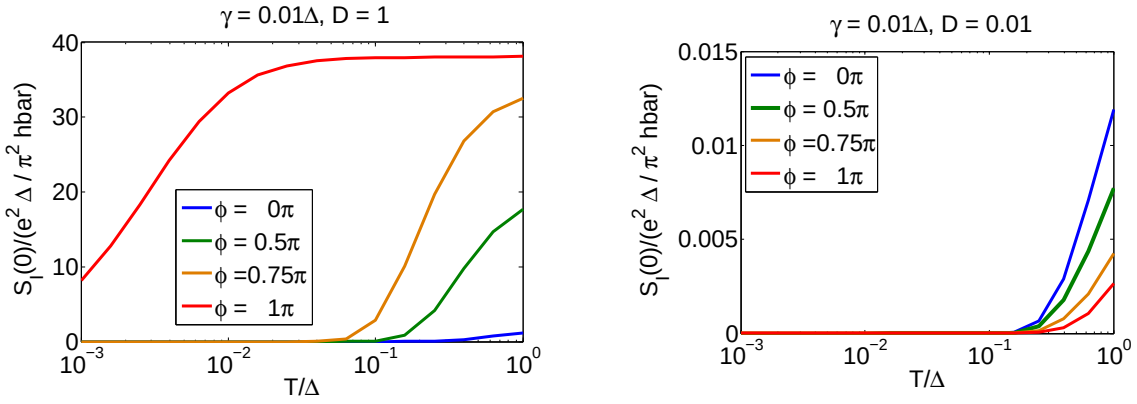

Figure 3.3: These plots show tthe emperature dependence of the zero-frequency noise for an open channel (Left) and a low transmission channel (Right).

For completeness, we study the noise as a function of the relaxation rate γ in figure 3.4. For a pinhole, the power law behavior of the noise confirms the Lorentzian character of the zero-frequency peak, as we increase γ the peak gets broader and smaller. As expected for that case, the current fluctuations are greater for $\phi = \pi$. As $D \to 0$, the bound state contribution to the noise is reduced and the later becomes almost γ independent. We also confirm that the maximal noise at low transmission is obtained at $\phi = 0$.

Therefore, we confirm that the zero-frequency noise is mostly influenced by the transmission eigenvalue of a channel and the phase difference across the two superconducting leads. In the case of tunnel junctions, the current fluctuations are almost independent of the temperature and the relaxation rate when $\gamma < T \ll \Delta$. Finally, let's note that figure 3.2 contains the information $S_I(\omega = 0, D)$ required by equation 3.4 to compute the noise over different realizations of disorder in superconducting nanodevices.

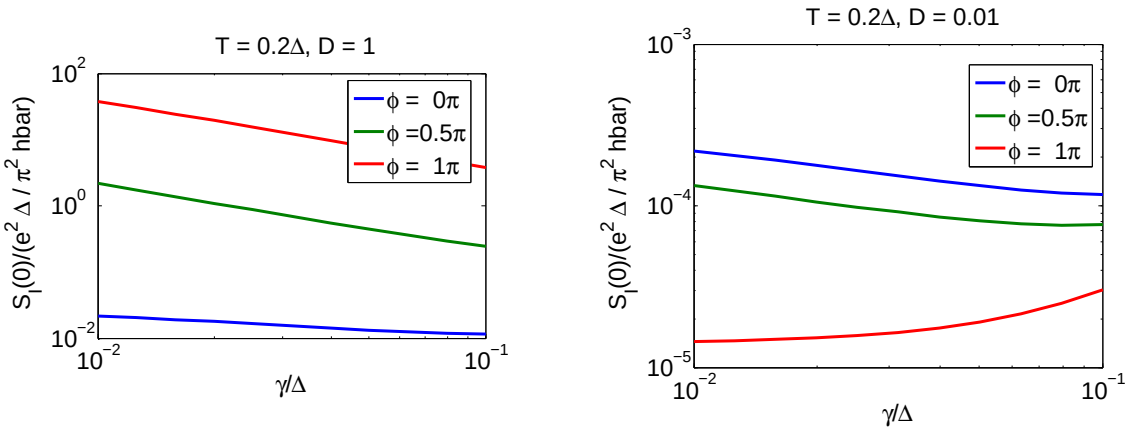

Figure 3.4: On the left side we have the effect of the relaxation rate on the low-frequency noise for an opened channel. The right side corresponds to a low transmission channel.

3.3 Chaotic Cavity

A chaotic cavity is a microstructure with an irregular geometry such that no particles are directly transmitted across the reservoirs. The time t_{dwell} spent by particles to cross a chaotic cavity is supposed much smaller than the time t_{ergodic} for the particle to acquire a random direction by bouncing off the boundaries of the structure. However, the dimensions of the cavity have to be small enough so that impurity scattering can be neglected and transport is assumed to be ballistic [28]. In some sense, a chaotic cavity is very analogous to a asymmetric (quantum) billiard table[29].

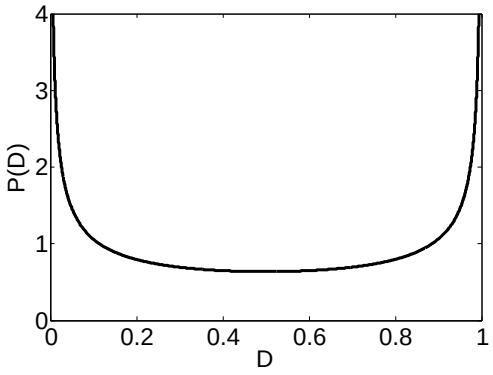

Figure 3.5: Probability density of transmission eigenvalues for a chaotic cavity.

The method that leads to the probability distribution of transmission eigenvalues of the scattering matrix $S = \begin{pmatrix} r & t' \\ t & r' \end{pmatrix}$ is random matrix theory, which is well described in [30] and [24]. The scattering matrix of a given chaotic cavity is a member of the circular unitary ensemble. This ensemble is defined through its invariant measure $d\mu(S) = d\mu(S')$ which remains constant under any transformation $S' = U_0 S V_0$, where U_0 and V_0 are some fixed unitary matrices. The matrices S are assumed to cover this matrix space with equal probability. A unitary scattering matrix can be parametrized as a function of D in the following way:

$$S = \begin{bmatrix} v^{(1)} & 0 \\ 0 & v^{(2)} \end{bmatrix} \begin{bmatrix} -\sqrt{1-\mathbf{D}} & \sqrt{\mathbf{D}} \\ \sqrt{\mathbf{D}} & \sqrt{1-\mathbf{D}} \end{bmatrix} \begin{bmatrix} v^{(3)} & 0 \\ 0 & v^{(4)} \end{bmatrix}, \tag{3.6}$$

where $\mathbf{D}$ is the $N \times N$ diagonal matrix of the $\{D_n\}$ and the $v^{(i)}$ are arbitrary unitary matrices. A differential arc length in this matrix space can be written as $d\sigma^2 = \text{Tr}\left(\text{dS}^\dagger \text{dS}\right)$.

Using a general property of measures on vector spaces, namely that for a differential arc length having the form $d\sigma^2 = \sum_{ab} g_{ab} dx^a dx^b$ we can write the volume measure $d\mu(V) = \sqrt{\det(\mathrm{g})} \prod_a dx^a$, we find that

$$d\mu(S) = P(\{D_n\}) \prod_a dD_a \prod_i d\mu\left(v^{(i)}\right). \tag{3.7}$$

The joint probability is identified to be

$$P(\{D_n\}) = C\exp\left\{-2\sum_{\mathrm{a<b}} \ln|\mathrm{D_a} - \mathrm{D_b}|\right\} \tag{3.8}$$

where C is a normalization constant. We remark that this has the form of the joint density in the global-maximum-entropy approach to transport in disordered systems [28]. Using the method of orthogonal polynomials in random matrix theory, the transmission eigenvalue density probability can be computed exactly using Legendre polynomials (because $0 < D < 1$). In the case where $N \to \infty$, one gets $P(D)$ such that

$$P(D) = \frac{1}{\pi\sqrt{D(1-D)}} \tag{3.9}$$

This probability distribution in plotted in figure 3.5 and can be integrated with no lower bound in the interval

$$0 < D < 1. \tag{3.10}$$

We notice this is a bimodal distribution symmetric around $D = \frac{1}{2}$ with equal weight in the low and high-transmission regimes, which implies $\langle D \rangle = \frac{1}{2}$. This distribution is also universal in the sense that it does not depend on parameters of the cavity.

The average noise and the sample-to-sample fluctuations can now be computed using equations 3.4 and 3.5. The results are shown in figure 3.6. We find that the zero-frequency noise in a chaotic cavity scales linearly with the number of channels N times a phase-dependent function. Indeed, the probability distribution 3.9 implies that the conductance of the junction should be proportional to the number of channels in the cavity, therefore noise scales with conductance in a chaotic cavity. However, the sample-to-sample fluctuations are shown to scale as $N^{-\frac{1}{4}}$ over a large range of channel numbers. Since computing the noise amounts to sampling the data in figure 3.2 with a fixed number of channels, the cavities with a few channels are expected to have more fluctuations in the relative number of high-noise pinholes than samples with a lot of channels and a rather constant fraction of pinholes.

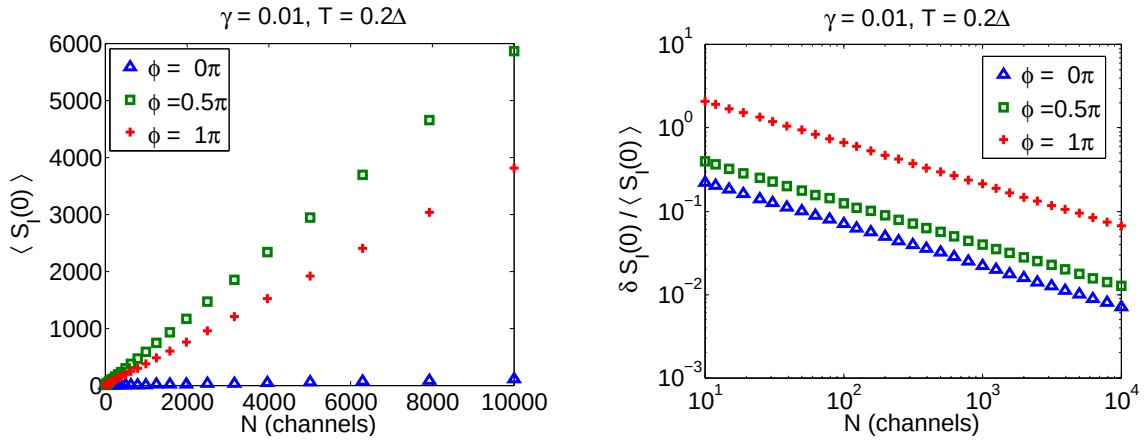

Figure 3.6: The average noise (Left) and the noise fluctuations (Right) of a chaotic cavity as a function of the number of channels are shown.

In figure 3.7, the phase-dependence of the average noise reveals that for all numbers of channels, the noise maximum is not at $\phi = \pi$ but rather somewhere between $0.8\pi < \phi < \pi$. Indeed, the few $D = 1$ pinholes only have a significant effect when $\phi = \pi$, but a large quantity of channels with $D < 1$ whose maximum noise is at a different phase contribute more significantly to the overall current fluctuations. The exact number of $D = 1$ pinholes is the main source of noise in the case $\phi = \pi$, therefore we observe that a fluctuation of this quantity can produce a large sample-to-sample fluctuation of the noise.

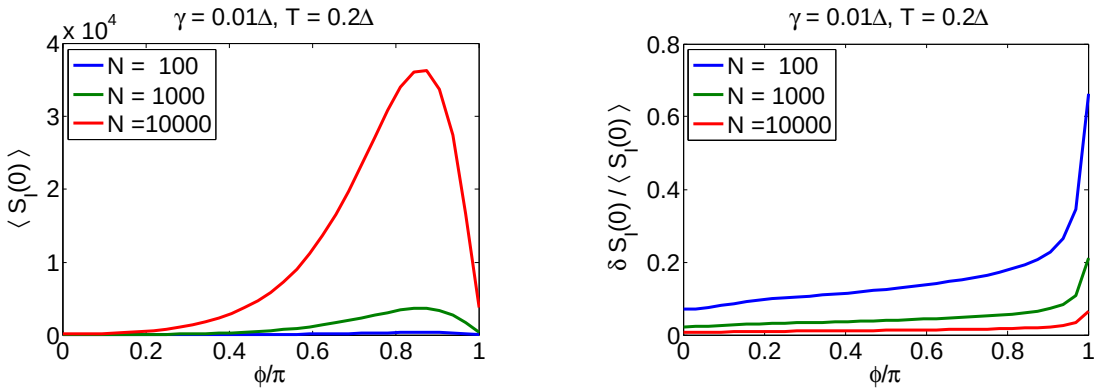

Figure 3.7: The phase-dependence of the average noise (Left) and its fluctuations (Right) of a chaotic cavity are shown.

3.4 Diffusive Wire

A diffusive conductor is a wire of length $L \gg \lambda_F$ such that $l \ll L \ll Nl$, where l is the mean free path of particles and Nl is the localization length [31]. In this case, the conductance of the wire diminishes linearly with increasing length $\langle G \rangle = G_0 \frac{Nl}{L}$ rather than exponentially as in the insulating regime. This implies that

$$1 \ll \langle G \rangle \ll N. \tag{3.11}$$

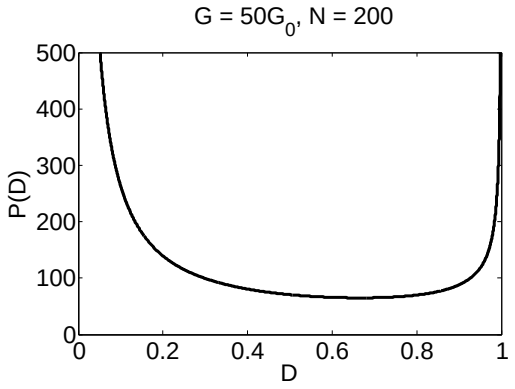

Figure 3.8: Probability density of transmission eigenvalues for a diffusive wire with a given conductance.

The usual approach to solve the diffusion problem in superconducting device is to use the Usadel equations [32]. If the system's dimensions are small enough such that there is no decay of superconductivity, diffusion can be described using ballistic channels with a relaxation mechanism which induces dephasing[18]. In our case, we model the wire as a set of ballistic point contacts connected through their transfer matrices M. The total transfer matrix is obtained by multiplying individual transfer matrices together such that the $2N$ eigenvalues of $MM^\dagger$ denoted $\mathrm{sech}^2(\mathrm{x_n})$ are uniformly distributed in the interval $\frac{L}{l} < x_n < \infty$. The resulting probability distribution is

$$P(D) = \frac{\langle G \rangle}{2D\sqrt{1-D}}. \tag{3.12}$$

As shown in figure 3.8, the probability distribution is bimodal. While most of the transmission channels have $D \ll 1$, a few of them are open at $D = 1$. The distribution can be

integrated in the interval

$$D_{min} = \mathrm{sech}^2 \frac{N}{\langle G \rangle} < D < 1 \tag{3.13}$$

such that $\int_{D_{min}}^{1} dDP(D) = N$. Therefore the distribution depends only on the total conductance $\langle G \rangle$ and well as the number of channels N.

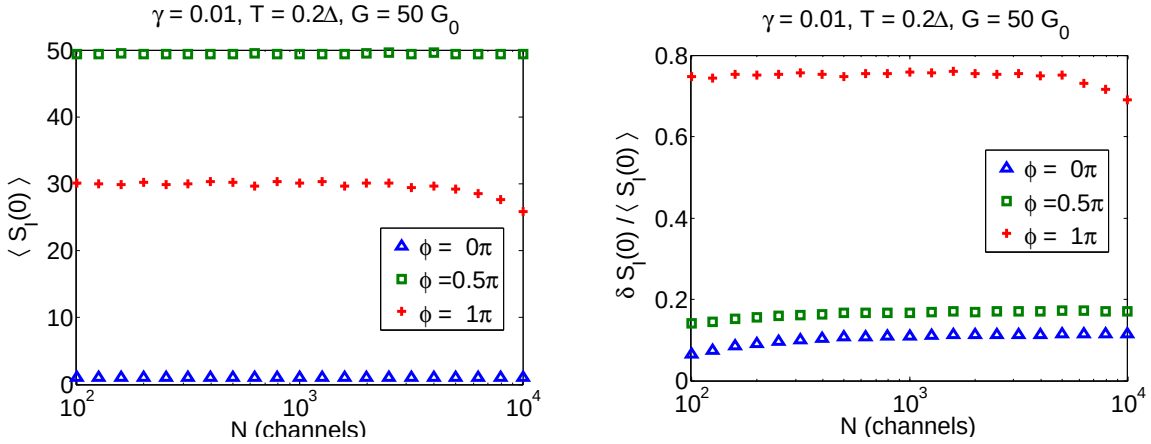

Figure 3.9: Average noise (Left) and noise fluctuations (Right) of a diffusive wire.

The noise and its sample-to-sample fluctuations are computed for a fixed value of the conductance while varying the number of channels. As shown in figure 3.9, the average noise is independent of the number of channels. The sample-to-sample fluctuations of the noise are also fairly flat functions of the number of channels. Therefore the noise in a superconducting wire and its reproducibility is only a function of the phase-dependent conductance.

The phase-dependence of the noise shown in figure 3.10 shows that the majority of the noise comes from partially opened pinholes and that the maximum is not at $\phi = \pi$. For a fixed conductance, the sample-to-sample fluctuations are most important at $\phi = \pi$ except when the number of channels becomes so high that only channels with $D < 1$ and no pinholes are needed to reach $\langle G \rangle$. In this case the sample-to-sample fluctuations range between 10% and 30% of the actual noise.

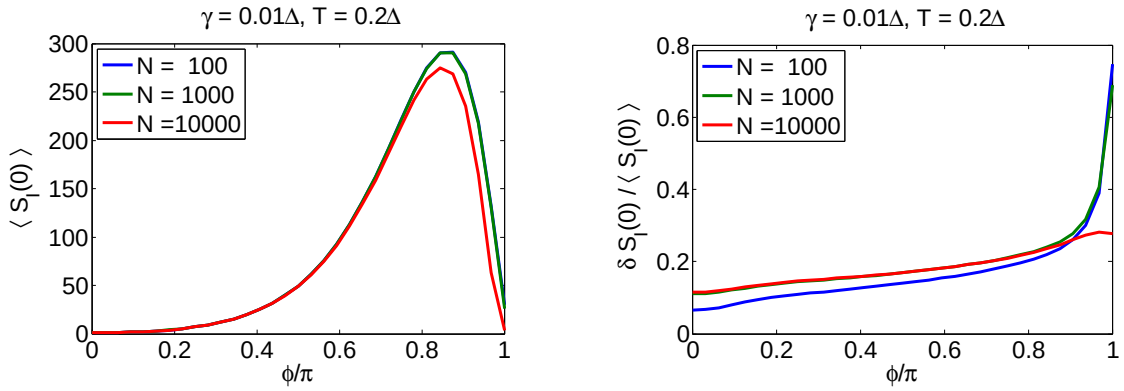

Figure 3.10: Phase-dependence of the average noise (Left) and its fluctuations (Right) of a diffusive wire.

3.5 Dirty Interface

Dirty interfaces are another class of universal disorder model [33][34]. In this case, the dimension of the zone where electron are strongly scattered is $L \ll \lambda_F$.

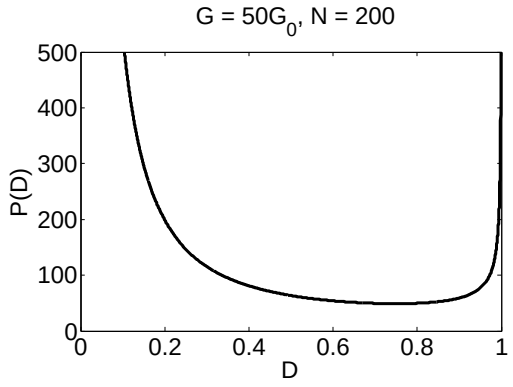

Figure 3.11: Probability density of transmission eigenvalues of a dirty interface.

To find the distribution of transmission eigenvalues of a dirty interface, it is first assumed that all states should lie near the Fermi level and that the short range scatterers modeled as delta functions are all located in a plane perpendicular to the transport direction. It can be shown that

$$tt^\dagger = \left[I + \tilde{\Gamma}\tilde{\Gamma}\right]^{-1}, \tag{3.14}$$

where t is the transmission matrix of propagating states and $\tilde{\Gamma}$ is the matrix of scattering amplitudes. Average quantities can be obtained from configurational averaging over all possible impurity positions. The analytical calculation of the distribution function is done by expanding t in powers of $\tilde{\Gamma}$. Two Ward identities can be found so that any product of t and $t^\dagger$ can be reduced to expressions containing only first order t and $t^\dagger$:

$$\begin{aligned} tt^\dagger &= \tfrac{1}{2}\left(t + t^\dagger\right) \\ tt &= \left(1 + m\tfrac{\partial}{\partial m}\right) t. \end{aligned} \tag{3.15}$$

The first comes from current conservation and continuity of the wave function across the interface. The second is less general and valid in the case of weak scattering regime where evanescent wave can be neglected or when $\tilde{\Gamma}$ is proportional to m (strong scattering regime). The model is not valid in the intermediate scattering regime.

The delta peaks of the probability distribution function are Fourier transformed and the exponential is expanded in powers of $tt^\dagger$. Using the Ward identities and a Kramers-Kronig relation, the distribution can be rewritten as a function of the conductance

$$\left\langle g\left(m^2\right)\right\rangle = \mathrm{Tr}\left\langle \mathrm{tt}^\dagger\right\rangle = \mathrm{Re}\left[\mathrm{Tr}\left\langle \mathrm{t}\right\rangle\right]. \tag{3.16}$$

The calculation of the distribution function is reduced a configurational averaging of t. A Green's function is introduced and a set of diagrams is obtained from the expansion in $\tilde{\Gamma}$. A Dyson equation is used to relate the configurationnally averaged Green's function to the unperturbed one and the self-energy. The conductance can then be computed from the Green's function and inputted back into the distribution function, which give the following result (see figure 3.11):

$$P(D) = \frac{\langle G\rangle}{\pi D^{3/2}\sqrt{1-D}}. \tag{3.17}$$

Specifically, this distribution is only valid in the strong scattering regime where

$$\langle G\rangle \ll N. \tag{3.18}$$

Again, this is a universal bimodal function which needs a low transmission cut-off

$$\frac{1}{1+\left(\frac{\pi N}{2\langle G\rangle}\right)^2} < D < 1 \tag{3.19}$$

such that $\int_{D_{min}}^{1} dDP\left(D\right) = N$.

The analysis of the noise of a strong scattering dirty interface is very similar to the case of a diffusive wire since both distribution functions have the same behavior near $D = 1$ and show a non-integrable singularity near when $D \to 0$. Indeed, in figure 3.12 we see that for a fixed conductance $\langle G\rangle$, the noise and the fluctuations remain fairly constant for all channel numbers.

Again, there is an exception for a large number of channels when $\phi = \pi$ because no pinholes are required for the interface to reach its full conductance and their influence is removed from the sample-to-sample noise fluctuations.

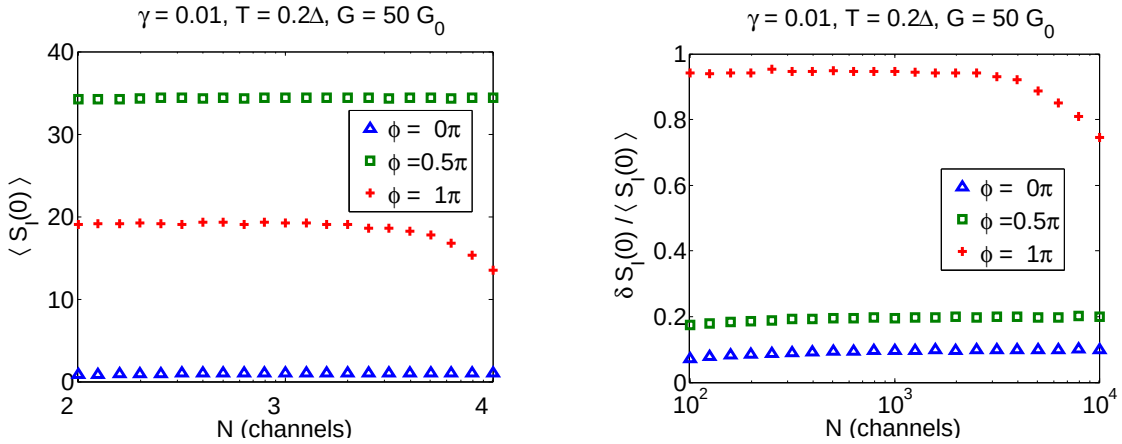

Figure 3.12: Average noise and noise fluctuations of a dirty interface.

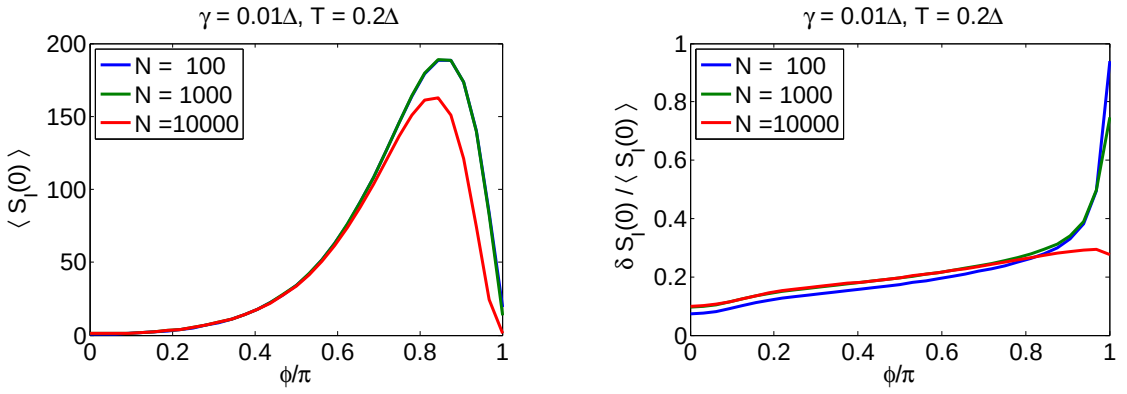

Figure 3.13: Phase-dependence of the average noise and its fluctuations of a dirty interface.

Chapter 4

Conclusion

By modelling the roughness of a junction as a set of channels with a bimodal distribution of transmission eigenvalues, the noise and its sample-to-sample fluctuations could be computed using the non-equilibrium many-body Green's function method.

The noise of a single channel is found to be strongly dependent on its transparency and the phase difference across its terminals. Channels set at $\phi = 0$ as well as low transmission channels $D \ll 1$ exhibit a shot noise spectrum at frequencies $\omega > 2\Delta$. Strong non-poissonian noise is found at low frequencies when $\phi = \pi$ for fully transmitting pinholes. This low frequency noise is induced by fast switching between states of opposing currents pinned at the Fermi level.

For different models of roughness with a few pinholes, the low frequency noise is found to be dominated by the partially transmitting channels. Experimentally, the roughness model could be confirmed by looking at the phase dependence of the noise of a single junction. From one sample to the other, the largest variation of the zero-frequency noise should be found at $\phi = \pi$ where the variation in the number of pinholes has the most impact.

References

[1] M. A. Nielsen and I. L. Chuang. *Quantum Computation and Quantum Information*. Cambridge University Press, 2000.

[2] D. P. DiVincenzo. The physical implementation of quantum computation, 2000.

[3] P. G. De Gennes. *Superconductivity of Metals and Alloys*. Westview Press, 1999.

[4] J. Clarke and F. K. Wilhelm. Superconducting quantum bits. *Nature*, 453:1031–1042, 2008.

[5] D. Averin and H. T. Imam. Supercurrent noise is quantum point contacts. *Physical Review Letters*, 76:3814–3817, 1996.

[6] A. Martin-Rodero, A. Levy Yeyati, F. J. Garcia-Vidal, and J. C. Cuevas. Comment on supercurrent noise in quantum point contacts, 1996.

[7] G. Heinrich and F. K. Wilhelm. Current fluctuations in rough superconducting tunnel junctions. *Physical Review B*, 80:214536, 2009.

[8] R. de Sousa, K. B. Whaley, T. Hecht, J. von Delft, and F. K. Wilhelm. Microscopic model of critical current noise in josephson-junction qubits: Subgap resonances and andreev bound states. *Physical Review B*, 80:094515, 2009.

[9] A. Martin-Rodero, A. Levy Yeyati, and F. J. Garcia-Vidal. Thermal noise in superconducting quantum point contacts. *Physical Review B*, 53:R8891R8894, 1996.

[10] Y. M. Blanter and M. Büttiker. Shot noise in mesoscopic conductors, 1999.

[11] R. J. Schoelkopf, A. A. Clerk, S. M. Girvin, K. W. Lehnert, and M. H. Devoret. Qubits as spectrometers of quantum noise, 2002.

[12] A. M. Zagoskin. *Quantum Theory of Many-Body Systems*. Springer, 1998.

[13] G. Rickayzen. *Green's Functions and Condensed Matter*. Academic Press, 1991.

[14] J. Rammer and H. Smith. Quantum field-theoretical methods in transport theory of metals. *Reviews of Modern Physics*, 58:323–359, 1986.

[15] W. Belzig, F. K. Wilhelm, C. Bruder, and G. Schön. Quasiclassical green's function approach to mesoscopic superconductivity. *Superlattices and Microstructures*, 25:1251–1288, 1999.

[16] A. I. Larkin and Y. N. Ovchinnikov. Nonlinear conductivity of superconductors in the mixed state. *Sov. Phys. JETP*, 41:960–965, 1976.

[17] I. O. Kulik and A. N. Omel'yanchuk. Josephson effect in superconductive bridges: microscopic theory. *Sov. J. Low Temp. Phys.*, 4:142–149, 1978.

[18] Y. V. Nazarov. Novel circuit theory of andreev reflection. *Superlattices and Microstructures*, 25:1221–1231, 1999.

[19] A. V. Zaitsev. Quasiclassical equations of the theory of superconductivity for contiguous metals and the properties of constricted microcontacts. *Sov. Phys. JETP*, 59:1015–1024, 1984.

[20] A. I. Larkin and Y. N. Ovchinnikov. Current damping in superconducting junctions with nonequilibrium electron dritribution functions. *Sov. Phys. JETP*, 60:1060–1067, 1984.

[21] A. V. Zaitsev. Theory of pure short s-c-s and s-c-n microjunctions. *Sov. Phys. JETP*, 51:111–117, 1980.

[22] V. A. Khlus. Current and voltage fluctuations in microjunctions between normal metals and superconductors. *Sov. Phys. JETP*, 66:1243–1249, 1987.

[23] C. W. J. Beenakker. Three "universal" mesoscopic josephson effects, 2004.

[24] C. W. J. Beenakker. Random-matrix theory of quantum transport. *Review of Modern Physics*, 69:731–808, 1997.

[25] S. Oh, K. Cicak, K. B. Cooper, K. D. Osborn, R. W. Simmonds, M. Steffen, J. M. Martinis, and D. P. Pappas. Low-leakage superconducting tunnel junctions with a single-crystal al_2o_3 barrier. *Superconductor science & technology*, 18:1396–1399, 2005.

[26] R. W. Simmonds, D. A. Hite, R. McDermott, M. Steffen, K. B. Cooper, K. M. Lang, J. M. Martinis, and D. P. Pappas. *Quantum Computing in Solid State Systems*, chapter Josephson Junction Materials Research Using Phase Qubits, pages 86–94. Springer, 2006.

[27] V. C. Hui and C. J. Lambert. Andreev scattering, universal conductance fluctuations and phase periodic transport. *Europhysics Letters*, 23:203–209, 1998.

[28] H. U. Baranger and P. A. Mello. Short paths and information theory in quantum chaotic scattering: transport through quantum dots. *Europhysics Letters*, 33:465–470, 1996.

[29] C. W. J. Beenakker. Andreev billiards, 2004.

[30] H. U. Baranger and P. A. Mello. Mesoscopic transport through chaotic cavities: A random s-matrix theory approach. *Physical Review Letters*, 73:142–145, 1994.

[31] M. J. M. de Jong and C. W. J. Beenakker. *Mesoscopic Electron Transport*, chapter Shot Noise in Mesoscopic Systems, pages 225–258. Kluwer Academic Publishers, 1997.

[32] T. T. Heikkilä, J. Särkkä, and F. K. Wilhelm. Suppercurrent-carrying density of states in diffusive mesoscopic josephson weak links. *Physical Review B*, 66:184513, 2002.

[33] K. M. Schep and G. E. Bauer. Transport through dirty interfaces. *Physical Review B*, 56:15860–15872, 1997.

[34] K. M. Schep and G. E. W. Bauer. Universality of transport through dirty interfaces. *Physical Review Letters*, 78:3015–3018, 1997.

[35] D. Averin and A. Bardas. Adiabatic dynamics of superconducting quantum point contacts. *Physical Review B*, 53:R1705–R1708, 1996.

[36] W. Belzig and Y. V. Nazarov. Full counting statistics of electron transfer between superconductors. *Physical Review Letters*, 87:197006, 2001.

[37] W. Belzig and Y. V. Nazarov. Full current statistics in diffusive normal-superconductor structures. *Physical Review Letters*, 87:067006, 2001.

[38] R. C. Bialczak, R. McDermott, M. Ansmann, M. Hofheinz, N. Katz, and E. Lucero. 1/f flux noise in josephson phase qubits. *Physical Review Letters*, 99:187006, 2007.

[39] G. E. Blonder, M. Tinkham, and T. M. Klapwijk. Transition from metallic to tunneling regimes in superconducting microconstrictions: Excess current, charge imbalance and supercurrent conversion. *Physical Review B*, 25:4515–4532, 1981.

[40] E. N. Bratus, V. S. Shumeiko, and E. V. Bezuglyi. dc-current transport and ac josephson effect in quantum junctions at low voltage. *Physical Review B*, 55:12666–12677, 1997.

[41] A. A. Clerk, M. H. Devoret, S. M. Girvin, F. Marquardt, and R. J. Schoelkopf. Introduction to quantum noise, measurement and amplification. *Review of Modern Physics*, 82:1155–1208, 2010.

[42] J. C. Cuevas and W. Belzig. Dc-transport in superconducting point contacts: a full counting statistics view. *Physical Review B*, 70:214512, 2004.

[43] M. H. Devoret, A. Wallraff, and J. M. Martinis. Superconducting qubits: A short review, 2004.

[44] P. Dieleman, H. G. Bukkems, T. M. Klapwijk, M. Schicke, and K. H. Gundlach. Observation of andreev reflection enhanced shot noise. *Physical Review Letters*, 79:3486–3489, 1997.

[45] P. Dutta and P. M. Horn. Low-frequency fluctuations in solids: 1/f noise. *Reviews of Modern Physics*, 53:497–516, 1981.

[46] K. B. Efetov. Random matrices and supersymmetry in disordered systems, 2005.

[47] A. V. Galaktionov, D. S. Golubev, and A. D. Zaikin. Statistics of current fluctuations at non-zero frequencies, 2003.

[48] D. S. Golubev and A. D. Zaikin. Coulomb interaction and quantum transport through a coherent scatterer. *Physical Review Letter*, 86:4887–4890, 2001.

[49] A. A. Golubov, M. Y. Kupriyanov, and E. Il'ichev. The current phase relation in josephson tunnel junctions. *Reviews of Modern Physics*, 76:411–469, 2004.

[50] S. Guéron. *Quasiparticles in a diffusive conductor: Interaction and pairing.* PhD thesis, CEA Saclay, 1997.

[51] D. J. Van Harlingen, T. L. Robertson, B. L. T. Plourde, P. A. Reichardt, T. A. Crane, and J. Clarke. Decoherence in josephson-junction qubits due to critical-current fluctuations. *Physical Review B*, 70:064517, 2004.

[52] Georg Heinrich. Full counting statistics of rough superconducting tunnel junctions. Master's thesis, Mnchen, 2007.

[53] A. Ingerman, J. Lantz, E. Bratus, V. Shumeiko, and G. Wendin. Andreev resonances in quantum ballistic transport in sns junctions. *Physica C*, 353:77–81, 2001.

[54] M. Kindermann and Y. V. Nazarov. Full counting statistics in electric circuits, 2003.

[55] J. S. Kline, H. Wang, S. Oh, J. M. Martinis, and D. P. Pappas. Josephson phase qubit circuit for the evaluation of advanced tunnel barrier materials. *Superconductor Science and Technology*, 22:015004, 2009.

[56] V. Lacquaniti, S. Maggi, E. Monticone, and R. Steni. Analysis of the interfaces of stacked josephson junctions by atomic force microscopy. *IEEE Transactions on Applied Superconductivity*, 7:2419–2422, 1997.

[57] K. M. Lang, D. A. Hite, R. W. Simmonds, R. McDermott, D. P. Pappas, and J. M. Martinis. Conducting atomic force microscopy for nanoscale tunnel barrier characterization. *Review of Scientific Instruments*, 75:2726–2731, 2004.

[58] K. M. Lang, S. Nam, J. Aumentado, C. Urbina, and J. M. Martinis. Banishing quasiparticles from josephson-junction qubits: Why and how to do it. *IEEE Transactions on Applied Superconductivity*, 13:989–993, 2003.

[59] H. S. Leff. Class of ensembles in the statistical theory of energy-level spectra. *Journal of Mathematical Physics*, 5:763–768, 1964.

[60] M. Lenander, H. Wang, R. C. Bialczak, E. Lucero, M. Mariantoni, M. Neeley, A. D. O'Connell, D. Sank, M. Weides, J. Wenner, T. Yamamoto, Y. Yin, J. Zhao, A. N. Cleland, and J. M. Martinis. Energy decay and frequency shift of a superconducting qubit from non-equilibrium quasiparticles, 2011.

[61] L. S. Levitov and H. Lee. Electron counting statistics and coherent states of electric current, 1996.

[62] V. F. Maisi, O.-P. Saira, Y. A. Pashkin, J. S. Tsai, D. V. Averin, and J. P. Pekola. Real-time observation of discrete andreev tunneling events. *Physical Review Letters*, 106:217003, 2011.

[63] J. M. Martinis. Superconducting qubits and the physics of josephson junctions, 2004.

[64] J. M. Martinis, M. Ansmann, and . Aumentado. Energy decay in josephson qubits from non-equilibrium quasiparticles, 2009.

[65] Y. V. Nazarov. Circuit theory of andreev conductance. *Physical Review Letters*, 73:1420–1423, 1994.

[66] Y. V. Nazarov and Y. M. Blanter. *Quantum Transport Introduction to Nanoscience*. Cambridge University Press, 2009.

[67] J. Salo, F. W. J. Hekking, and J. P. Pekola. Frequency-dependent current correlation functions from scattering theory. *Physical Reviews B*, 74:125427, 2006.

[68] V. S. Shumeiko, E. N. Bratus, and G. Wendin. Scattering theory of superconductive tunneling in quantum junctions. *Low Temperature Physics*, 23:181, 1993.

[69] R. W. Simmonds, K.M. Lang, D. A. Hite, S. Nam, D. P. Pappas, and J. M. Martinis. Decoherence in josephson phase qubits from junction resonators. *Physical Review Letters*, 93:077003, 2004.

[70] R. de Sousa, K. B. Whaley, F. K. Wilhelm, and J. von Delft. Ohmic and step noise from a single trapping center hybridized with a fermi sea. *Physical Review Letters*, 95:247006, 2005.

[71] M. Tinkham. *Introduction to Superconductivity*. McGraw-Hill, Inc., 1996.

[72] M. B. Weissman. 1/f noise and other slow, nonexponential kinetics in condensed matter. *Reviews of Modern Physics*, 60:537–571, 1988.

[73] F. C. Wellstood, C. Urbina, and J. Clarke. Flicker (1/f) noise in the critical current of josephson junctions at 0.094.2 k. *Applied Physics Letters*, 85:5296–5298, 2004.

[74] F. K. Wilhelm, M. J. Storcz, U. Hartmann, and M. R. Geller. Superconducting qubits ii: Decoherence, 2006.

[75] A. V. Zaitsev. Erratum: Theory of pure short s-c-s and s-c-n microjunctions. *Sov. Phys. JETP*, 52:1018, 1980.

[76] A. Zazunov, V. S. Shumeiko, E. N. Bratus, J. Lantz, and G. Wendin. Andreev level qubit. *Physical Review Letters*, 90:087003, 2003.